UNCLASSIFIED

AD 419024

DEFENSE DOCUMENTATION CENTER

FOR

SCIENTIFIC AND TECHNICAL INFORMATION

CAMERON STATION, ALEXANDRIA, VIRGINIA

UNCLASSIFIED

NOTICE: When government or other drawings, specifications or other data are used for any purpose other than in connection with a definitely related government procurement operation, the U. S. Government thereby incurs no responsibility, nor any obligation whatsoever; and the fact that the Government may have formulated, furnished, or in any way supplied the said drawings, specifications, or other data is not to be regarded by implication or otherwise as in any manner licensing the holder or any other person or corporation, or conveying any rights or permission to manufacture, use or sell any patented invention that may in any way be related thereto.

64-5

CATALOGED BY DDC
AS AD No. 419024

AIR FORCE INSTITUTE OF TECHNOLOGY

AIR UNIVERSITY
UNITED STATES AIR FORCE

419024

SCHOOL OF ENGINEERING

WRIGHT-PATTERSON AIR FORCE BASE, OHIO

AF-WP-O-OCT 63 3,500

DETERMINATION OF A SINGLE POINT ON THE HUGONIOT SOLID EQUATION OF STATE CURVES

George Philip Grotewell, Jr.

GNE/Phys/63-6

AF-WP-O-SEP 63 25

DETERMINATION OF A SINGLE POINT ON THE HUGONIOT SOLID EQUATION OF STATE CURVE

THESIS

Presented to the Faculty of the School of Engineering of
the Air Force Institute of Technology
Air University
in Partial Fulfillment of the
Requirements for the Degree of
Master of Science

By
George Philip Crotwell, Jr., B.S. E.E.
1/Lt. USAF
Graduate Nuclear Engineering
August 1963

Preface

This thesis is experimental in nature with the aim of securing data on Pressure vs Compressibility for several materials. I have tried to present a general description of the experiments and a brief discussion of the theory behind the experiments in language such that readers with varied technical backgrounds may understand it.

The references give more specific detail about the theory to anyone who desires such information. For more detail information about the experimental procedure, the Air Force Special Weapons Center located at Kirtland AFB, New Mexico should be contacted.

I am deeply indebted to a number of persons for their assistance in completing my thesis. I cannot mention all of them individually, but I do wish to mention two by name. I acknowledge my sincere appreciation to the personnel of the Physics Division, AFSWC, who made this work possible and particularly to Alc Henry Lawrence for his long hours of helpful assistance in perfecting the experiment and to Dr. W. L. Lehman, my faculty advisor, for his constructive criticism of my thesis.

George P. Crotwell, Jr.

Contents

Contents

List of Figures

List of Figures

List of Tables

List of Tables

List of Symbols

Symbol	Definition
P_o	Sample Pressure in Shock-Free Material
P	Sample Pressure in Shocked Material
P_q	Quartz Pressure
ρ_o	Sample Density in Shock-Free Material
ρ	Sample Density in Shocked Material
ρ_q	Quartz Density
Co	Sound Wave Propagation Velocity in Sample at Zero Particle Velocity
Co_q	Sound Wave Propagation Velocity in Quartz at Zero Particle Velocity
U_o	Sample Particle Velocity in Shock-Free Material
U	Sample Particle Velocity in Shocked Material
η	Compressibility (Ratio: ρ/ρ_o)
D	Shock Propagation Velocity in Sample Material
α	Transmission Factor
i(t)	Quartz Output Current
A	Area of Inner Electrode
K	Piezoelectric Constant
v_x	Shock Propagation Velocity in Quartz
h	Quartz Crystal Thickness
P_q (o,t)	Pressure at Front of Quartz Crystal

List of Symbols

Symbol	Definition
P_q (h,t)	Pressure at Back of Quartz Crystal
V	Transducer Output Voltage
T	Sample Thickness
tt	Shock Wave Transit Time Through Sample
W	Sabot Velocity
E	Relative Error

Abstract

The Hugoniot solid equation of state curve is the curve of pressure and compressibility for a sample material. Compressibility, η, is the ratio of the densities of the shocked material to that of the shock-free material. The shock wave creating the pressure is produced by forcing an aluminum sabot down the barrel of a light gas gun to impact on a pressure transducer. The light gas gun has the desirable ability to reproduce sabot velocities and to produce planar impacts.

The theory behind the experiments is in two parts. One part relates the pressure produced on impact to compressibility through the following two equations.

$$P = \rho_o DU \qquad (A)$$

$$\rho_o D = \rho (D-U) \qquad (B)$$

The other relates the pressure incident on the transducer to its electrical output. This relationship is given in the next equation.

$$i(t) = \frac{AKv_q}{h} \left[(P_Q(o,t) - P_q(h,t) \right] \qquad (C)$$

The quartz method and deceleration Hugoniot method of determining η as a function of pressure give two approaches to the problem. The quartz method uses the electrical output of the transducer to determine the pressure and then uses the first equation to obtain U. η is determined now that U is known. The deceleration Hugoniot method relates

the particle velocity of the sample to that of the sabot and graphically determines pressure and particle velocity of the sample material. η is then calculated.

The pressure transducer assembly is composed of a lucite holder, a sample material, and a quartz crystal. The piezoelectric property of the quartz converts the pressure to electrical output. Besides measuring the pressure, the propagation velocity of the shock wave in the sample, the velocity of the sabot, and the planarity of impact are also determined in each shot.

The relative experimental error of the results is less than 2.8% for the quartz method and less than 4.1% for the deceleration method. The results from both methods are combined to give a single point on the Hugoniot solid equation of state curve. These centroid values of the individual shots has a maximum relative experimental error of 7% and are given as follows: C-124: P= 9.17 K bar, η = 1.093; Chopped nylon filled phenolic: P = 8.40 K bar, η = 1.094; Oblique tape wound refrasil: P = 7.74 K bar, η = 1.075; Carbon: P = 14.32 K bar, η = 1.044; Gold: P = 39.49 K bar, η = 1.020; and Teflon: P = 10.37 K bar, η = 1.163.

GNE/Phys/63-6

DETERMINATION OF A SINGLE POINT ON THE HUGONIOT SOLID EQUATION OF STATE CURVE

I. Introduction

The purpose of this thesis is to determine a point on the Hugoniot solid equation of state curve for several different re-entry vehicle materials. The experiments were designed to simulate low kilobar* pressure impacts in the 0-20 kilobar range and primarily around ten. (10) kilobar.

The Hugoniot solid equation of state is defined as the curve of Pressure vs Compressibility. Compressibility, η, is defined as the ratio of the density of the material just behind the shock front to the density of the material before the shock front or the ratio of the density of the shocked material to that of the shock-free material.

At present, little data is available on the shape and value of the Hugoniot equation of state curve in this pressure region for these re-entry materials. Hence, determination of a single point on the curve in this pressure range is of great value in interpolation and prediction of events which utilize the Hugoniot solid equation of state.

The shock waves are generated by use of a 2 1/2" light gas gun which propels a projectile, termed a sabot, at controlled velocities which impacts on the sample being investigated. The gas gun shown in Fig 1-1 represents an excellent step forward in equation of state

* 1 bar = 10^6 dynes/cm^2 $\sim$ 1 atmosphere

investigation in that it can reproduce sabot velocities (i.e. shocks) to a much higher degree of accuracy than other means, such as exploding foils and high explosives. Just as important as its ability to reproduce velocities is the feature of producing extremely planar impacts. This is a definite advantage over the other means of producing shocks.

Fig 1-1

Gas Gun Assembly

To obtain the necessary pressure profiles and pressures generated by the impacting sabot, a quartz pressure transducer technique is utilized. By use of this transducer, composed of a sample R-V material and quartz crystal mounted in a lucite holder, these desired objectives are obtained.

Six materials are used in the experiments. They are gold, teflon, chopped nylon filled phenolic (CNP), Castable 124 (C-124), oblique tape wound refrasil (OTWR), and pyrolytic graphite (P-G). The gold and teflon are used to represent the basic materials. Gold is used because of its high atomic number and teflon is representative of the plastics. CNP, C-124, OTWR, and P-G are the engineering materials used.

CNP is a homogenious mixture of chopped nylon fiber randomly dispersed in a phenolic binder. C-124 is a homogenious solid of epoxy. OTWR is a fiberglass tape in a phenolic binder, and of course, P-G is carbon. These engineering materials are representative of most ablation materials used in re-entry vehicles.

The results obtained from the experiments tie down points on the equation of state curves for CNP, OTWR, P-G, C-124, and Au. The results for teflon are inconclusive and vary considerably outside experimental error limits.

The basic theories for the experiments, and consequently this thesis, are presented in Chapter 2. It briefly explains the sources for the equations of state, how they are used, and what parameters are measured to render these equations solvable.

Chapter 3 deals with the experimental procedure. It gives the objectives of the experiments, describes the apparatus and instrumentation, and gives the procedure used to perform a single experiment. A sample calculation, error analysis, and brief discussion of the results and experiments in general are given in Chapter 4. A thorough presentation of these results in the form of graphs and tabulated numerical values is given in Appendix D.

The experiment was conducted at Kirtland Air Force Base, New Mexico, under the supervision of the Physics Branch of the Air Force Special Weapons Center. The experimental work was done in-house using the newly completed facilities of the Physics Laboratory. The theory background was supplied by the Physics Analysis Section and Sandia Corporation which has pioneered the quartz technique.

II. Theory

Introduction

The objects of this section are to present the basic theories on which the experiments are based and to discuss the methods used to determine the Hugoniot solid equation of state curve. The experiments are designed to determine η , defined as the ratio of the density of the shocked material to the density of the shock-free material, ρ/ρ_o , as a function of pressure creating the shock wave. The pressure is produced by impacting a sabot travelling at a high velocity against the sample.

Two brief theoretical discussions are presented in the first two sections; one relates P to η and the other relates the electrical output of a quartz transducer to the pressure incident on the transducer. The last sections present the quartz and deceleration Hugoniot methods of determining the Hugoniot solid equation of state curve.

Hugoniot Solid Equation of State

The equations of state, which relate the pressures, densities, and particle velocities, on either side of a shock wave, are presented in the following section.

Fig 2-1 represents a shock wave AB propagating toward the right with a velocity D in a material in the laboratory frame of reference.

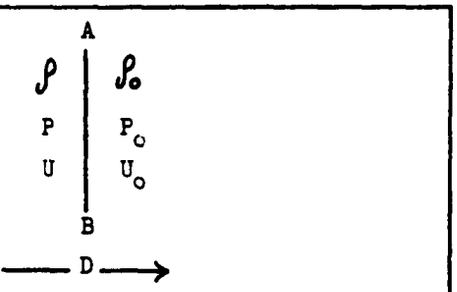

Fig. 2-1

Schematic of Shock Wave Propagation

The pressure, density, and particle velocity in the shock-free material (i.e. before the shock wave) are designated by Po, ρ_o, and Uo respectively. Po and Uo are both zero in this region. The pressure, density, and particle velocity in the shocked material, (i.e. behind the shock wave) are designated as P, ρ, and U respectively. P and U are no longer zero.

It is more convenient to work in the frame of reference in which the shock wave AB is at rest. In this frame, the particle velocity before the shock wave is Vo = D - Uo = D. The particle velocity behind the shock wave is V = D - U. The mass flow, the product of density and particle velocity, must be the same before and behind the shock wave. This results in the first equation of state:

$$\rho_o D = \rho (D - U) \quad \text{or} \quad \eta = \frac{D}{D-U} \qquad (1)$$

By Newton's Laws, the pressure difference, P - Po must equal the change in momentum per unit area per unit time. This yields the second equation of state:

$$P - P_o = -\rho(D-U) \quad (D-U) + (\rho_o D) \quad D = \rho_o DU \qquad (2)$$

A purely mathematical derivation of these equations of state is given by Courant and Friedrichs (Ref 1) and a physical derivation is discussed by G. E. Dwall (Ref 2).

Quartz Transducer

In Fig 2-2, A is the sample material, B is the quartz crystal, and C is the lucite holder. The heavy line between the sample A and the quartz B represents a thin copper foil used as an electrode. The lines D, E, and F are electrical outputs from the quartz crystal.

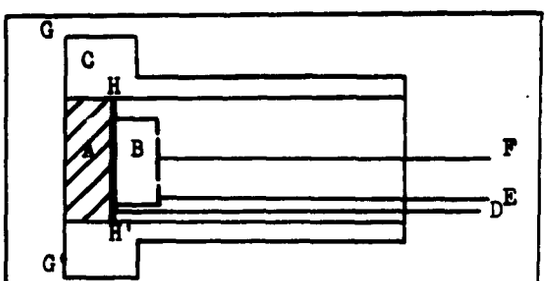

Figure 2-2

Quartz Transducer

The impact of the sabot on the surface GG' produces a shock which propagates through the sample and passes through the copper foil into the quartz. Because of its piezoelectric properties, the quartz crystal produces a current proportional to the stress in the crystal during the

period while the shock wave propagates through the crystal. This stress, due to the shock wave, will persist over the time interval (t) required for the shock wave to reach the back of the crystal. The stress in the quartz is dependent on the pressure difference between HH' and the back. The equation for current as a function of time is given by (Ref 7:3226):

$$i(t) = \frac{AKv_q}{h} \left[P_q(o,t) - P_q(h,t) \right] \qquad (3)$$

where:

A = active electrical area

K = piezoelectric constant

v_q = shock propagation velocity in quartz

h = thickness of quartz crystal

$P_q(o,t)$ = pressure at front of quartz

$P_q(h,t)$ = pressure at back of quartz

The above discussion assumes that a square shock wave is produced when the sabot impacts on the transducer. This assumption is good because the close tolerance of the barrel and sabot insure a planar impact. However, as the shock propagates through the R-V material, it is dispersed somewhat and no longer is a definite square wave. Another assumption is that over the time period ($\sim 1.1\,\mu$sec) that measurements are made, the pressure behind the shock wave is constant in time. This second assumption is valid since the time required for a rarefaction wave to return to the quartz is twice the transit time ($\sim 2\,\mu$sec)

through the R-V material. Hence, all measurements are made before the rarefaction can effect the reading. The guard rings eliminate the effects of transverse pressure build-up from the sides of the crystal so the center electrode is subject to the actual pressure incident on its front surface. The effects eliminated by the guard rings is discussed in Appendix A.

Determination of Equation of State Curve

There are two methods of determining a point on the Hugoniot curve. They use the two equations of state, a known Hugoniot curve of the sabot material, the pressure P, the shock wave propagation velocity D, sabot velocity W, and the quartz current output equation.

Quartz Method

By measuring P and D and knowing the initial density of the sample ρ_o, Eq (2) is used to determine U. Eq (1) yields η as a function of D and U and, therefore, the point on the Hugoniot curve, P vs η, has been determined.

To measure D, the impact of the sabot on the transducer triggers an oscilloscope at time, (t_o). The input to the scope is from the outside quartz electrode (i.e. the area outside the guard ring) and will produce no current until the shock propagates through the sample and enters the front of the quartz crystal at time (t_x). When the shock enters the quartz, the scope trace is deflected and the transit time, ($tt = t_x - t_o$), thus is determined. By measuring the sample

thickness, T, before the shot, the propagation velocity D can be determined from:

$$D = \frac{T}{tt} \tag{4}$$

To determine the pressure in the sample which has been designated P, the pressure in the quartz crystal, P_q, is calculated from Eq (3). P and P_q are related by a transmission factor, α, discussed later.

We are only interested in the pressure difference between the front and back surface of the crystal during the time in which the shock wave propagates through the crystal. Thus, the pressure of the back of the crystal, P_q (h,t) will be zero. The output current of the quartz produces a voltage across the input scope resistance, R_s. By measuring the voltage, the pressure in the quartz is determined from Eq (5):

$$P_q(o,t) = \frac{V(t)}{\frac{AKv_q}{h} R_s} \tag{5}$$

where:

$V(t) = i(t) \cdot R_s$ = output voltage

Due to the reflections at the interface HH' in Fig 2-2, the pressure in the quartz is related to the pressure in the sample by:

$$P_q = \alpha P \tag{6}$$

The transmission factor, α, is given by Eq (7) (Ref 11,93):

$$\alpha = \frac{2 \rho_{o_q} C_{o_q}}{\rho_{o_q} C_{o_q} + \rho_o C_o} \tag{7}$$

where:

ρ_{o_q} = density of quartz

ρ_o = density of sample material

C_{o_q} = sound wave velocity in quartz at zero particle velocity

C_o = sound wave velocity in sample at zero particle velocity

P is used in Eq (2) to obtain U. Now knowing D and U, Eq (1) yields η. The sample pressure is then plotted against the appropriate values of η to yield the Hugoniot equation of state curve.

Deceleration Method (Ref 13)

As in the quartz method, the wave propagation velocity D must be measured. This parameter is the common quantity used in both methods of determining the Hugoniot curve.

The sabot velocity W is necessary and is measured by use of pins. This procedure is described in the experimental section.

The value of D is determined for each shot. Eq (2) states that the point on the P vs U curve corresponding to the particular value of D lies somewhere on the straight line whose slope is (ρ_o D).

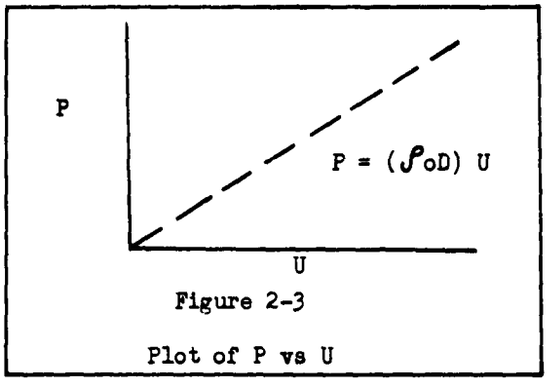

Figure 2-3

Plot of P vs U

Fig. 2-3 is the frame of reference in which the sample is at rest.

The sabots are made of AL-6061-T6; and the curve of P vs U is well-defined for this grade of aluminum.

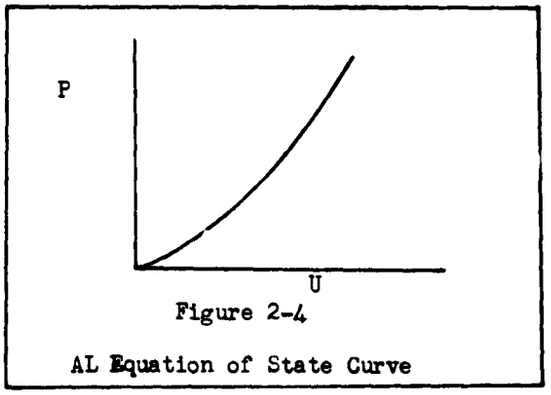

Figure 2-4

AL Equation of State Curve

Fig. 2-4 illustrates this curve in the frame of reference in which the aluminum sabot is at rest. This frame of reference is moving with a velocity W, relative to the sample. This curve of P vs U for AL-6061-T6 is plotted in Appendix C.

In the frame of reference of the sample, the aluminum particle velocity is the velocity of the sabot and the sabot pressure is zero until impact. On impact a decelerating pressure is imparted to the sabot and the aluminum particle velocity decreases. A plot of P vs U

for the aluminum in the frame of reference of the sample, yields a mirror image of the P vs U curve in Fig 2-4, but shifted by the sabot velocity W, Fig 2-5.

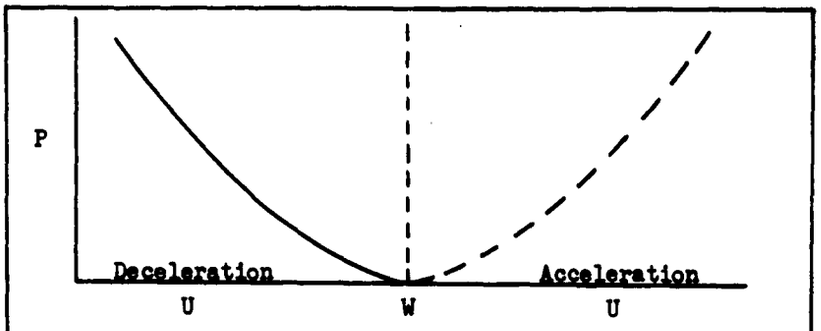

Figure 2-5

Deceleration AL Equation of State Curve

At the interface the aluminum and sample particle velocities are the same. Hence, by superimposing the deceleration Hugoniot curve on the straight line plot of P vs U in Fig 2-3, the intersection of the two curves is the only particle velocity that will satisfy the condition that particle velocity is constant across an interface. The corresponding pressure and particle velocity at the intersection is the sample pressure P and sample particle velocity U. P, U, and D now have been determined for one specific shot so η can be calculated from Eq (1) and one point on the sample's Hugoniot equation of state curve has been determined.

For another shot, another value of W, and corresponding D is obtained. The procedure is repeated with the deceleration Hugoniot curve shifted to a new value of W.

In this manner, a P vs U curve and, in turn, a P vs η curve is determined for the sample material.

III. Experimental Procedure

Introduction

An aluminum sabot is forced down the barrel of a light gas gun by high pressure. Velocity pins, inserted in the side of the barrel, are shorted by the sabot as it passes. The sabot then impacts on an instrumented pressure transducer assembly producing a shock wave (i.e. pressure) in the transducer assembly. A diagram of this arrangement, called the light gas gun, is shown below.

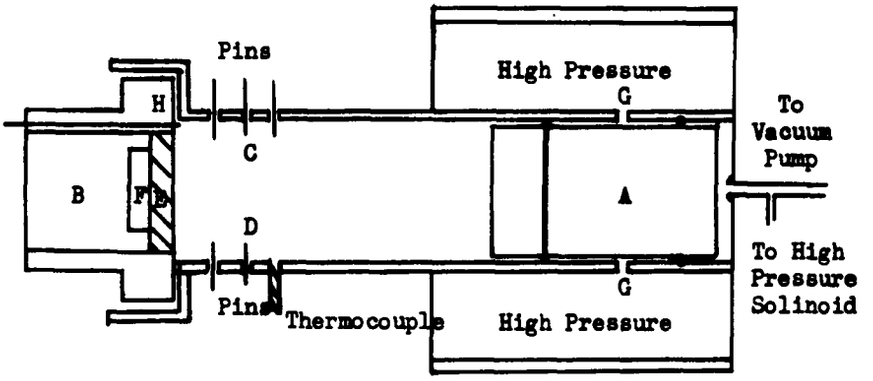

Figure 3-1

Schematic of Light Gas Gun Assembly

The aluminum sabot is placed in position A and the transducer is placed in position B in above diagram (Fig 3-1). The volume behind and in front of the sabot is evacuated to approximately 10 microns. Velocity pins and a vacuum monitoring thermocouple are placed in positions C and D. The breech is pressurized to a pre-determined pressure to produce the desired velocity when fired.

The vacuum behind the sabot is dumped, or more specifically, the breech pressure is introduced to the volume behind the sabot through a high pressure solenoid valve. This forces the sabot forward past the orifices, G, which permits the chamber pressure in the breech to accelerate the sabot down the barrel to the desired velocity. The sabot shorts out the velocity pins at C and D and from these pins its velocity, W, can be determined. The sabot then impacts on the target which is a transducer assembly, B. This consists of a lucite holder, sample material, and quartz crystal. The planarity pins in the lucite holder at H determine the flatness of impact.

The impact of the sabot on the transducer produces a shock wave which propagates through the sample E and quartz crystal F. Measuring the transit time between impact and the emergence of the shock from the back of the sample allows the shock propagation velocity in the R-V material to be calculated. The piezoelectric effect of the quartz crystal, F, produces a current proportional to the incident pressure on it; hence, the pressure and its profile are measured by the quartz crystal.

From the preceding discussion, the following parameters must be measured on each shot; (a) velocity of the sabot, (b) planarity of impact, (c) shock wave propagation velocity, and (d) quartz pressure and its profile. Measurement of each of these parameters will be discussed individually later.

Transducer Assembly

The pressure transducer assembly which converts the shock pressure to electrical output is composed of three primary parts and their associated electronic leads. The three parts are: (a) the lucite holder, (b) the sample material, and (c) the quartz crystal. The pressure transducer is shown below in Fig 3-2 and each of its primary parts is discussed individually in the following paragraphs.

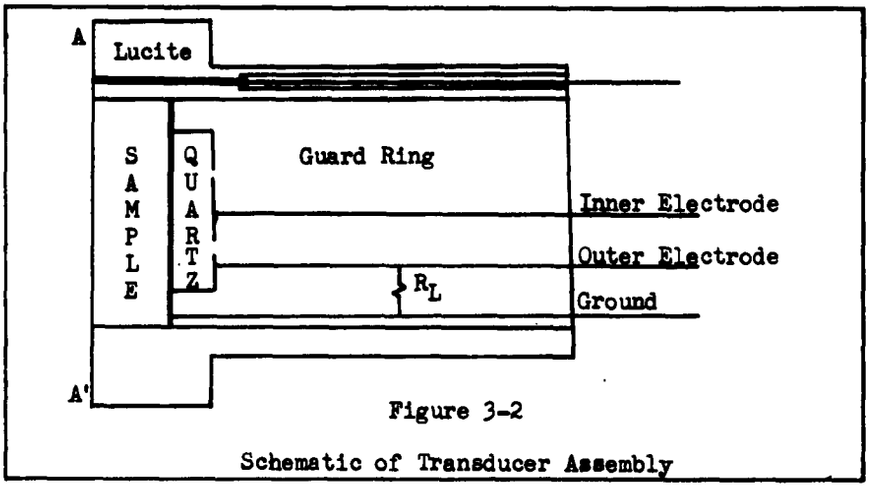

Figure 3-2

Schematic of Transducer Assembly

Lucite Holder. The lucite holder has a three fold purpose. First, it provides a sturdy rigid container for the sample and quartz crystal and allows them to be potted in epoxy resin to yield a flat front surface AA' of the transducer assembly in Fig 3-2. Second, it is a simple method of attaching the transducer assembly to the barrel of the gas gun. Third, it provides for radial placement of the planarity pins. The first and second purposes need no explanation. The third purpose is discussed because of its direct relation to planarity measurements.

The planarity pins are placed on a 2-5/32" diameter circle, spaced 120° radially. The pins are machine screws with the ends rounded to prevent arcing to the sabot and are set flush with the front surface of the lucite holder. The pins are made flush by placing the holder in contact with a flat steel plate and setting the screws so that electrical continuity is obtained between the pins and the plate (Ref 12:7). Epoxy is poured around the pins to give a vacuum seal.

Sample Material. The sample material is machined as a cylindrical slab as shown below.

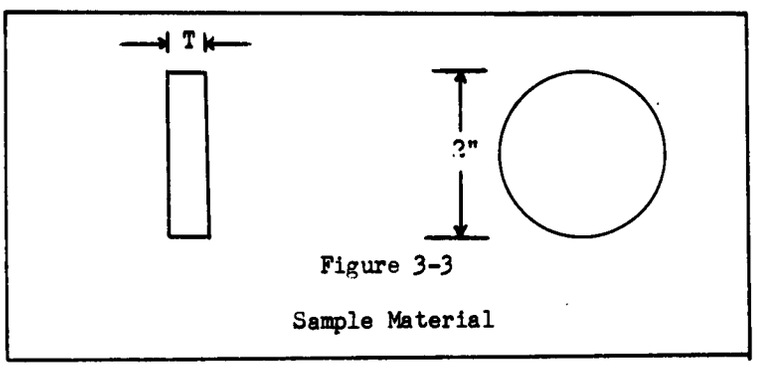

Figure 3-3

Sample Material

The diameter of this is held to ± .05" to insure a good fit in the lucite holder. The thickness T is approximately 1/4" and is not critical. However, it is extremely critical that the thickness varies less than ± .001", which insures that the faces of the sample are flat. A thin copper foil is bonded to the sample which serves as the ground electrode and a lead is soldered to this electrode.

Quarts Crystal. The quartz crystals are shown in Fig 3-4.

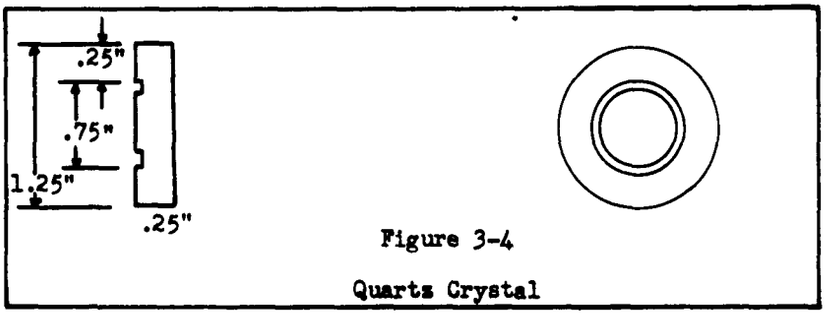

Figure 3-4

Quarts Crystal

The crystals are gold plated and this plating serves as a collecting electrode. A guard ring (See Appendix B) is cut in the positive face of the crystal just deep enough to cut the gold plating. This produces an inner and outer electrode. Leads are soldered to the two electrodes to carry the current produced by the quartz.

Velocity

To determine velocity the transit time over known distances (i.e. between velocity pins) is measured. The velocity pins are shown in Fig 3-5.

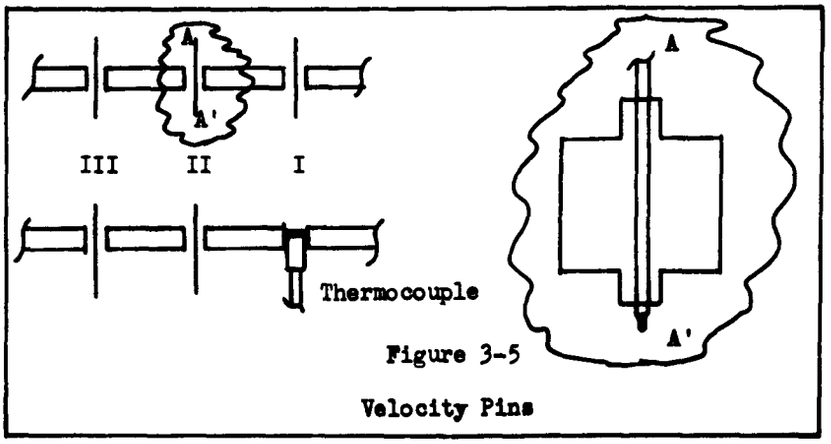

Figure 3-5

Velocity Pins

The insulated wire is shaved at the tip to allow the sabot to short-out an element of a R-C circuit. Shorting pin I produces a pulse which can be used to trigger two counters. Using the pin II pulse to stop one of the counters and the pulse from pin III to stop the second counter, the transit times between pins I and II and pins I and III is measured. Since the pin holders were machined to extremely close dimensions the distance between the pins is known. Therefore, the velocity of the sabot is simply the distance between the pins divided by the transit time between the respective pins.

One of the bottom holders is used for a thermocouple to monitor the barrel vacuum; therefore, only two pins are inserted on the bottom and only one velocity measurement is obtained from the bottom pins. The final pin that is shorted on the bottom, pin III (bottom), also serves to trigger another counter which is combined with a pulse from the planarity circuit (to be discussed later), to give the transit time between pin III (bottom) and the transducer. Measuring the distance between these two points determines the velocity of the projectile again.

Thus, the velocity of the sabot was determined between four sets of reference points.

V pins I-II (top)

V pins I-III (top)

V pins II-III (bottom)

V pin III - transducer

The average of these four readings is taken to be the velocity of the sabot.

Planarity

The sabot shorts the three planarity pins A, B, and C, shown in Fig 3-6, discharging the capacitors of a R-C circuit.

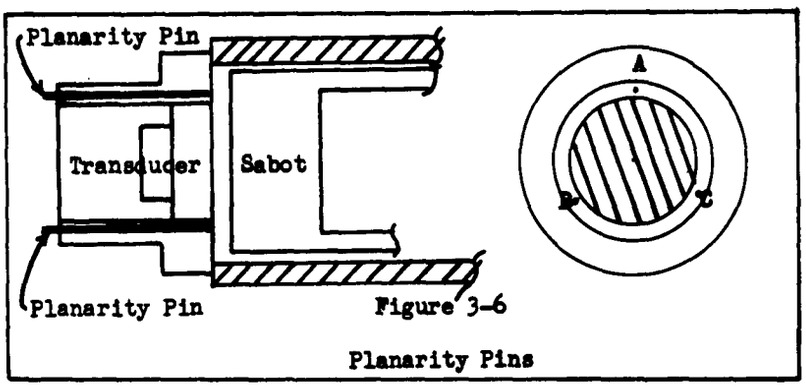

Figure 3-6

Planarity Pins

The pulse from the first pin to be shorted by the sabot triggers the oscilloscope. Pulses from the second and third pins show up as breaks in the scope trace. A fifty megacycle sine wave is placed on the bottom of the trace for a time reference. The time from the start of the trace to the last pulse is the closure time. Closure time is the time it takes the sabot surface to come in complete contact with the surface of the transducer. Closure times less than 500 nano sec are considered good since from the geometry, the closure time across the inner electrode area of the sample (3/4" diameter) would be about 1/3 of the total closure time.

A closure time of 500 ns would indicate a tilt of about .15 mm between the sabot and the lucite holder and a tilt of .05 mm between the sabot and the inner electrode sample surface for the velocities used in the experiments.

Wave Propagation Velocity

In Fig 3-7 the sabot A impacts on the first planarity pin E and produces a pulse which triggers an oscilloscope.

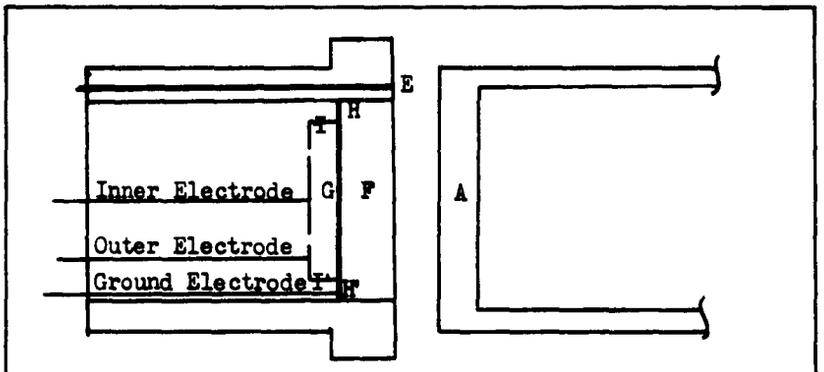

Figure 3-7

Pressure Transducer
(Wave Propagation Velocity Measurement)

The shock wave generated by the impact of the sabot propagates through the sample F. When the shock emerges from the back of the sample it strikes the quartz crystal G which immediately produces a current output. This signal from the outside electrode is used as input to the scope. The interval of time between the start of the scope trace and the input from the quartz is the transit time of the shock through the sample. A twenty megacycle sine wave is placed on the bottom of the trace as a time reference. This gives time resolution of less than .05 micro sec. By previously determining the thickness of the sample and measuring the transit time, the shock propagation velocity can be calculated.

Quartz Pressure

The sabot impacts on the transducer assembly generating a shock wave which propagates through the sample. It enters the quartz crystal and introduces pressure on the face of the crystal, HH', in Fig 3-7. The pressure at the rear of the crystal, II', is zero so the crystal is under compression (i.e. a stress is introduced). The quartz crystal generates current proportional to the stress, and this current produces a voltage across the scope resistance R_s. The voltage trace on the scope is called the pressure profile. The scope is calibrated prior to the shot so the quartz output (voltage) is measured. Eq (5) relates this voltage to the incident pressure on the face of the crystal HH' so the pressure in the quartz is measured.

Procedure

The procedure used to perform the experiment is divided into four parts:

1. Preparation of Transducer Assembly
2. Instrumentation and Scope Calibration Check-Out
3. Gun Set-Up
4. Fire and Recording of Data

A brief discussion of the important elements of each part of the procedure follows.

Preparation of Transducer Assembly. The three essential elements of the transducer assembly are assumed to be on hand. The guard ring is cut in the positive face of the crystal by a sandblaster and small jig. This jig and sandblaster arrangement cuts a circular groove, .004" wide, whose diameter is 3/4".

Measurements are made of sample thickness, quartz crystal thickness, guard ring width, and the inside diameter of the guard ring. A thin copper foil, 2 mils thick, is bonded to the sample and then the negative face of the quartz crystal is bonded to this copper foil. Leads are soldered to the inner and outer electrode of the quartz crystal and a ground lead is soldered to the copper foil.

The sample, crystal, and leads are put in the lucite holder and this transducer assembly positioned in a potting jig. This jig holds the assembly flush against a flat steel plate. Planarity pins are set and the transducer assembly is potted in epoxy resin to make it rigid and to give a vacuum seal.

Instrumentation and Scope Calibration Check-Out. A Rutherford generator is used to simulate the electrical signals produced by a shot. A pulse is sent down the planarity line and a delayed square wave is introduced in the quartz line and wave propagation velocity lines. These simulated pulses allow for an operational check of the scopes which determine the planarity, the quartz pressure, and the wave propagation velocity. The velocity counters are checked by shorting the velocity pins which also checks the pins and the R-C circuit.

After all instruments have been checked, a known D. C. voltage is introduced in the quartz transmission lines to calibrate the entire system.

Gun Set-Up. The barrel of the gun is swabbed clean and the sabot is positioned in the breech. A vacuum is drawn behind the sabot. The velocity pins are positioned in the barrel. The transducer is placed on the end of the barrel and the barrel is evacuated to about 10 microns. The transducer leads are connected to their respective transmission lines and any vacuum leaks are plugged with vacuum sealer. The catcher, which stops the sabot, is filled with plywood and aluminum hexcel.

Fire and Record. The breech is pressurized to a predetermined pressure by high pressure nitrogen bottles. A final check is made to insure that all scopes are set. The shutters on the scopes are then opened and the gun is fired. The shutters are closed, and the photographic results are removed from the cameras. All counters are recorded immediately.

IV. Results

There are four purposes for this chapter. First, a sample calculation is presented to show how the data obtained from the shots is used in the theoretical equations to yield the Hugoniot equation of state curve. The second topic is an error analysis to give the reliability of the results. The third purpose is to give tabulated results for the six sample materials tested. Fourth, a general discussion of the discrepancies is presented.

Sample Calculation

In the following discussion all measurements were obtained from a specific shot (Shot #82) on C-124 sample material. This particular shot is chosen because it is representative of all the shots and clear photographs were obtained for the data.

Most of the data obtained from the experiments is recorded on photographs. Hence, an extremely important part of a calculation is the interpretation of these photos. This data reduction is discussed first followed by a complete sample calculation using both methods described in Chapter II.

Data Reduction. Photographs of the data as recorded in Shot #82 with C-124 as the sample material is shown in Fig 4-1.

A is a photograph of the quartz output voltage or the pressure profile of C-124. The lines at the top of the photo are the voltage calibration lines. B shows the transit time of the shock wave through

the sample. There is a 20 megacycle sine wave on the bottom of the picture for time calibration. C depicts the pulses produced by the planarity pins as they are individually shorted by the sabot. The sine wave below that trace has a 50 megacycle frequency.

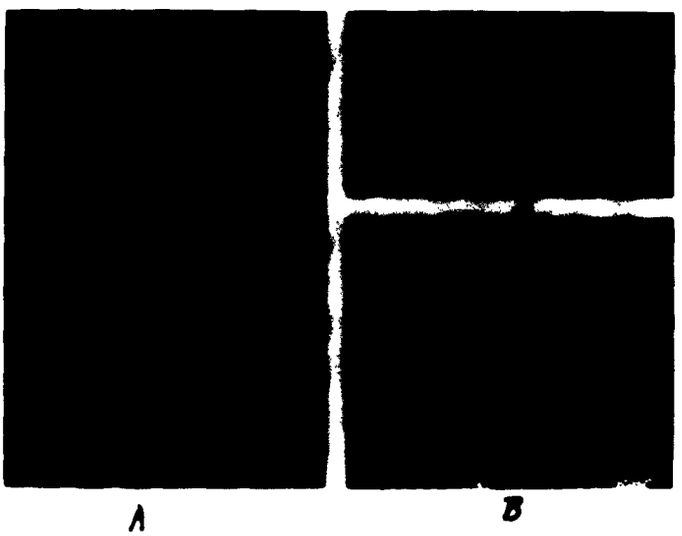

To obtain the magnitude of the voltage produced by the transducer, the relative distance between the base line and the front edge of the trace, AB, is measured as shown in Fig 4-2.

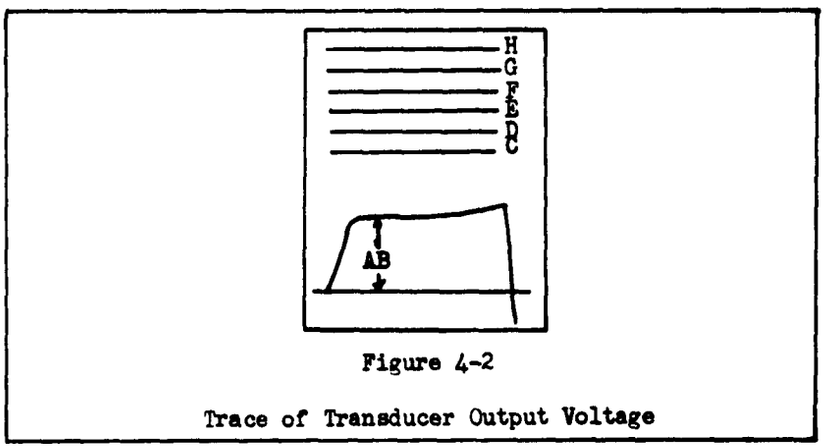

Figure 4-2

Trace of Transducer Output Voltage

Then the distance between the base line C (V = 0 volts) and the calibration lines is measured (i.e. CD, CE, CF, CG, CH), where

CD = 1 X 5 volts

CE = 2 X 5 volts

CF = 3 X 5 volts

CG = 4 X 5 volts

CH = 5 X 5 volts

The distance which represent 5 volts, $\overline{CL}$, is defined as:

$$\overline{CL} = \frac{CD + CB + CF + CG + CH}{15} \tag{8}$$

Then, V, the output voltage of the transducer is:

$$V = \frac{AB}{\overline{CL}} \quad X\ 5 \text{ volts} \tag{9}$$

The wave propagation velocity was obtained in a similar manner. As shown in B, Fig 4-1, the transit time of the shock wave through the sample is the time lapse between the start of the scope trace and the point at which the trace leaves the base line.

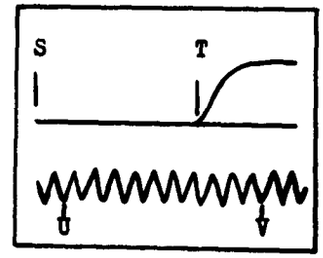

Figure 4-3

Trace of Wave Transit Time

By measuring the distance ST shown in Fig 4-3, the relative distance for this transit time is established. Measuring the relative distance for 10 cycles of the 20 megacycle sine wave UV, the distance proportional to 0.5 μ sec is obtained. The transit time is:

$$tt = \frac{ST}{UV} \times 0.5 \ \mu \text{ sec} \qquad (10)$$

Since the planarity of impact is not used in any of the calculations, the simple process of counting the number of cycles between the start of the trace and the pulse produced by shorting of the last planarity pin and converting this number of cycles to time is used. This determined the closure time with a resolution of 20 nano sec since a 50 megacycle time reference is used. This method gave a good indication of the planarity of impact.

The velocity of the sabot, W, is easily calculated. The travel time of the sabot is measured between points a known distance apart so the velocity is determined. Travel times, respective distances, and their associated velocities are given in Table 4-1.

Table 4-1
Sabot Velocity Values for Shot #82

Points	Travel Time (μ sec)	Distance (ft)	W (ft/sec)
Pins I-II (top)	103.9	0.100	962.5
Pins I-III (top)	207.9	0.200	962.0
Pins II-III (bottom)	104.0	0.100	961.5
Pin III - Transducer	253.9	0.244	961.0
TOTAL			3847.0
AVE			961.7

$\bar{W} = 0.02933$ cm/ μ sec

Computation - Quartz Method. For these calculations the values measured in Shot #82, and constants used in the equation are listed in Appendix E.

From Eq (4), D is determined:

$$D = \frac{T}{tt}$$

$$= \frac{0.7401 \text{ cm}}{2.58 \ \mu\text{sec}} = 0.2870 \text{ cm}/\ \mu\text{sec}$$

From Eq (5), P_q is obtained:

$$P_q = \frac{V}{\frac{AKv_q}{h} R_s} = 15.8 \text{ K bar}$$

where:

$V = 46.92$ volts

$A = \frac{\pi (\text{G-R Dia})^2}{4} = 2.85 \text{ cm}^2$

$K = 2.16 \times 10^{-8}$ coul/cm^2 - K bar

$v_q = 0.572 \text{ cm}/\ \mu\text{sec}$

$h = 0.6312$ cm

$R_s = 54\ \Omega$

Eq (6) yields P:

$$P = \frac{P_q}{\alpha_{C-124}} = \frac{15.8 \text{ K bar}}{1.718} = 9.22 \text{ K bar}$$

where: $\alpha_{C-124} = 1.718$

U is determined from Eq (2) now that P and D have been calculated:

$$U = \frac{P}{\rho_o D} = \frac{9.22 \times 10^{-3} \quad \frac{gm - cm}{\mu sec} \, cm^2}{(1.24 \ gm/cm^3)\ (.287 \ cm/\mu sec)} = 0.0259 \ cm/\mu sec$$

where:

$$\rho_o \ C\text{-}124 = 1.24 \ gm/cm^3$$

and

$$1 \text{ K bar} = 10^9 \text{ dynes/cm}^2 = 10^{-3} \quad \frac{gm - cm}{sec^2} \Big/ cm^2$$

η is calculated from Eq (1) now that D and U are known:

$$\eta = \frac{D}{D-U} = \frac{0.287 \ cm/\mu sec}{(0.287 - 0.0259) \ cm/\mu sec} = 1.10$$

The desired results - P, U, and η - have been determined and plots of P vs U, P vs η, and D vs U can be made.

Computation-Deceleration Method. The actual values of P and U for a given shot lie on the straight line whose slope is ($\rho_o D$). Since D has been calculated and ρ_o (C-124) is known, the point lies somewhere on the dashed line plotted in Fig 4-4, P = ($\rho_{o_{C-124}}$ D) U.

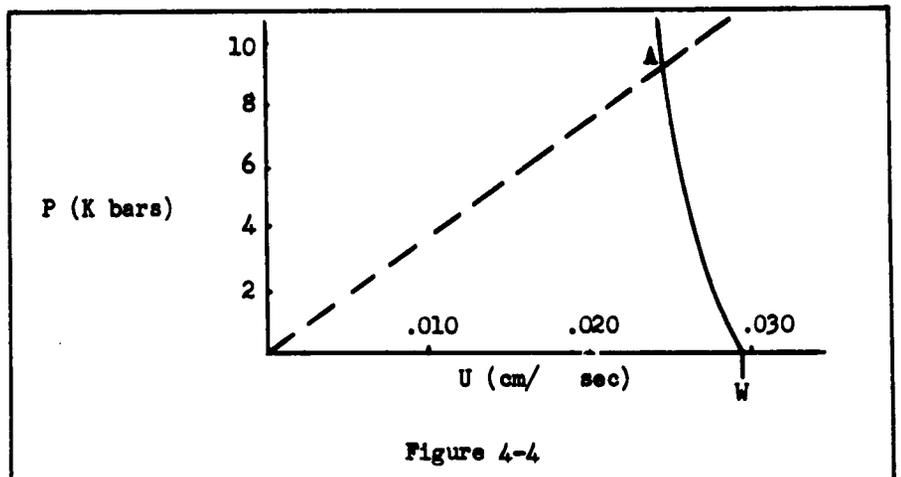

Figure 4-4

Intersection of Sample Hugoniot Curve and Aluminum Hugoniot Curve

The plot of the deceleration Hugoniot curve of aluminum given in Appendix C is placed such that its mirror image projects on Fig 4-4 with its origin at W. W is obtained from Table 4-1. The intersection of the two curves at A is determined and corresponding particle velocity and pressure of this point are read P = 8.59 K bar and U = 0.0241 cm/μ sec. These are the desired values of P and U. Eq (1) yields η now since D and U are known:

$$\eta = \frac{D}{D-U} = \frac{.287 \text{ cm}/\mu \text{ sec}}{(.287 - .0241 \text{ cm}/\mu \text{ sec}} = 1.09$$

The quantities P, η, and U have been determined and can be presented graphically.

Error Analysis

In an experimental thesis there are a great many sources of error which effect the results. The following discussion will evaluate the errors observed in this thesis and give an overall experimental error. This discussion will deal with the measurement of sample thickness, quartz thickness, quartz guard-ring diameter, wave transit time, quartz output voltage, sabot velocity, and the statistical error obtained when combining several shots to give a single point on the Hugoniot equation of state curve. Each of these errors will be discussed individually. The total error is evaluated by using the following equations (Ref 1:29-43):

$$E = (E_a^2 + E_b^2 + E_c^2)^{1/2} \tag{11}$$

where:

E = total error

E_a = individual error

$$O_a = \left(\sum \frac{(X-\bar{X})^2}{N} \right)^{1/2} \tag{12}$$

where:

O_a = standard deviation of a

X = experimental value of a

$\bar{X}_a$ = average value of a

N = number of experimental values of a

$$E_a = \frac{O_a}{\bar{X}_a} \times 100\% \tag{13}$$

Sample Thickness. The measured values of T are given in Table 4-2.

Table 4-2
Values of C-124 Sample Thickness for Shot #82

Reading	T (cm)	$(T-\bar{T})$ cm	$(T-\bar{T})^2$ cm^2
1	7.400	.001	.000001
2	7.396	.005	.000025
3	7.408	.007	.000049
TOTAL	22.204		.000075
AVE	7.401		

$$\sigma_T = \frac{.000075}{3}^{1/2} = 0.005 \text{ mm}$$

$$E_T = \frac{0.005 \text{ mm}}{7.401 \text{ mm}} \times 100\% < 0.1\%$$

Quartz Crystal Thickness. The measured values of h are given in Table 4-3:

Table 4-3
Values of Quartz Crystal Thickness for Shot #82

Reading	h (mm)	$(h-\bar{h})$ mm	$(h-h)^2$ mm^2
1	6.416	.004	.000016
2	6.414	.002	.000004
3	6.406	.006	.000036
TOTAL	19.236		.000056
AVE	6.412		

$$\sigma_h = \frac{.000056}{3}^{1/2} = 0.0043 \text{ mm}$$

$$E_h = \frac{0.0043 \text{ mm}}{6.412 \text{ mm}} \times 100\% < 0.1\%$$

Quartz Guard Ring Diameter. The measured values of G-R Dia are given in Table 4-4.

Table 4-4
Values of Quartz Guard Ring Diameter for Shot #82

Reading	G-R Dia (mm)	$(G-\bar{G})$ mm	$(G-\bar{G})^2$ mm^2
1	19.012	.024	.000576
2	19.059	.023	.000526
TOTAL	38.071		.001102
AVE	19.036		

$$\sigma_{GR\ Dia} = \frac{.001102 \text{ mm}^2}{2}^{1/2} = 0.0235 \text{ mm}$$

$$E_{GR\ Dia} = \frac{0.0235 \text{ mm}}{19.036 \text{ mm}} \times 100\% < 0.2\%$$

Wave Transit Time. The 20 megacycle sine wave time reference shown in Fig 4-3 gives a resolution of 1/2 cycle or 0.025 μ sec. Hence, even for the shortest transit times (1.35 μ sec), the error as a percent of tt is:

$$E_{tt} = \frac{0.025 \ \mu\text{sec}}{1.35 \ \mu\text{sec}} \times 100\% < 1.8\%$$

Quartz Output Voltage. Several factors influence the V measurement. They are the errors created in obtaining the calibration distance for 5 volts and in reading the voltage distance AB as shown in Fig. 4-2. Tables 4-5 and 4-6 give the values observed for these qualities for Shot #82.

Table 4-5
Value of Calibration Distance Per 5 Volts for Shot #82

Reading	A Number of 5 Volt Distances Represented	X Distance (Arbitrary Units)	$\bar{Y}$ (A·X)	$(\bar{Y}-X)$	$(\bar{Y}-X)^2$
1	1	52.0	52.7	.7	.49
2	2	106.0	105.4	.6	.36
3	3	158.0	158.1	.1	.01
4	4	210.0	210.8	.8	.64
5	5	265.0	263.5	1.5	2.25
TOTAL		791.0			3.75
AVE		52.7			

$$\sigma_c = \frac{3.75}{5}^{1/2} = 0.85$$

$$E_c = \frac{0.85}{52.7} \times 100\% < 1.6\%$$

Table 4-6
Values of Pulse Height (Voltage Distance AB, Fig 4-2) for Shot #82

Reading	Distance (Arbitrary Units)	$(X-\bar{X})$	$(X-\bar{X})^2$
1	491.0	3.8	14.4
2	505.0	10.2	104.0
3	490.0	4.8	23.0
4	490.0	4.8	23.0
5	498.0	3.2	10.2
TOTAL	2474.0		174.6
AVE	494.8		

$$\sigma_d = \frac{174.6}{5}^{1/2} = 5.9$$

$$E_d = \frac{5.9}{494.8} \times 100\% < 1.2\%$$

The relative error in V then is:

$$E_v = (E_c^2 + E_d^2)^{1/2}$$

$$= ((1.6)^2 + (1.2)^2)^{1/2} < 2.0\%$$

Sabot Velocity. Sabot velocity determination is dependent on the time lapse between two points and the distance between these two points. This time lapse is greater than 100 μ sec for all the experiments and the counters used to read this time lapse have a resolution of 0.1 μ-sec. Hence, the relative error in travel time of the sabot is:

$$E_s = \frac{0.1\ \mu\text{sec}}{100\ \mu\text{sec}} \times 100\% < 0.1\%$$

Since the pins are set at precise points, the absolute error in distance between the two pins reduces to the bending of the tips of the pretruding wires shown in Fig 3-5. These wires pretrude a maximum of 0.01 ft. and the distance between pin holders was 0.1 ft. If the pins are bent so that they compliment each other in increasing the absolute error as shown in Fig 4-5, the maximum absolute error is 2d.

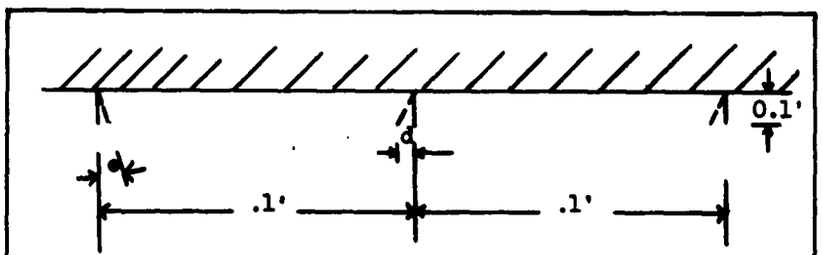

Figure 4-5

Schematic of Velocity Pins

The maximum value of angle θ to pass undetected is about 10°.

$$2d = (2)\ (.01 \sin 10^\circ)$$
$$= (2)\ (.01)(.18) = 0.0036'$$

The relative error in distance is:

$$E_i = \frac{0.0036'}{.1'} \times 100\% < 3.6\%$$

The error in W then is

$$E_w = (E_s^2 + E_i^2)^{1/2}$$
$$= ((.1)^2 + (3.6)^2)^{1/2} < 3.7\%$$

Graphical Interpretation. The values of P and U used in the deceleration method are read from the intersection of the two curves shown in Fig 4-4. P is accurate to 0.005 K bar and U is correct to 0.00005 cm/ μ sec. The relative errors in P and U for the minimum values of these quanities are:

$$E_p = \frac{0.005 \text{ K bar}}{5.00 \text{ K bar}} \times 100\% < 0.1\%$$

where:

$$P_{min} = 5.00 \text{ K bar}$$

$$E_u = \frac{0.00005 \text{ cm/ } \mu\text{sec}}{0.01660 \text{ cm/ } \mu\text{sec}} \times 100\% < 0.3\%$$

where:

$$U_{min} = 0.01660 \text{ cm/ } \mu\text{sec}$$

The relative error in the graphical readings is:

$$E_g = (E_p^2 + E_u^2)^{1/2}$$

$$= ((.1)^2 + (.3)^2)^{1/2} < 0.4\%$$

Statistical Error. This error is important when a single point for a specific sample material is desired from a number of individual points. Plots of these points are given in Appendix D. A least square curve was fitted to the points for minimum error in both ordinate and abscissa quantities. Eq (11) and Eq (12) are used to give the statistical error given below for C-124.

E_{se} = 2.7% for the P vs U curve

E_{se} = 4.1% for the P vs η curve

E_{se} = 2.7% for the D vs U curve

The least square curve fit, statistical error, and centroid of the points were programmed for the IBM 1620 Computer but since these operations are quite simple and straight-forward, no write-up of the program is included in the thesis.

Total Experimental Error. The total relative experimental error in the quartz method include the errors in sample thickness, quartz crystal thickness, quartz guard-ring diameter, wave transit time, and quartz output voltage.

$$E_{\text{quartz}} = (E_T^2 + E_h^2 + E_{\text{G-R Dia}}^2 + E_{tt}^2 + E_v^2)^{1/2}$$

$$= ((.1)^2 + (.1)^2 + (.2)^2 + (1.8)^2 + (2.0)^2)^{1/2} < 2.8\%$$

The individual errors that make up the relative experimental error in the deceleration method are errors in sample thickness, wave transit time, sabot velocity, and graphical interpretation.

$$E_{\text{deceleration}} = (E_T^2 + E_{tt}^2 + E_w^2 + E_g^2)^{1/2}$$

$$= ((.1)^2 + (1.8)^2 + (3.6)^2 + (.4)^2)^{1/2} < 4.1\%$$

Tabulated Results

The following results were obtained for C-124, CNP, OTWR, P-G, Au, and teflon.

Table 4-7
Values of D, P, U and η for the Sample Materials

Material	D (cm/μsec)	P (K bar)	U (cm/μsec)	η
C-124	0.2941	9.17	.0251	1.093
CNP	0.2846	8.40	.0242	1.094
OTWR	0.2659	7.74	.0185	1.075
P-G	0.3962	14.32	.0165	1.044
Au	0.3228	39.49	.0064	1.020
Teflon	0.1972	10.37	.0249	1.163

These values represent the centroid of the individual points obtained from the shots made on each material. The centroid is defined as the intersection of the two least square lines for minimum error in the abscissa and ordinate. Fig 4-6 illustrates the centroid of the P vs U curve for C-124.

The error limits shown for the centroid are the result of combining experimental error with the statistical error. The experimental error is taken as 4% for both methods which yields slightly larger error limits than would be obtained if points from each method are treated separately. For this shot the following error limits are:

$$E_{tot} = (E_{exp}^2 + E_{se}^2)^{1/2}$$

$$= (4.0^2 + 2.7^2)^{1/2} = 4.8\%$$

where:

$E_{se} = 2.7\%$ for P vs U

Tabulated values of D, P, U and η for individual shots for the samples are listed in Appendix D. Statistical and total errors are also listed.

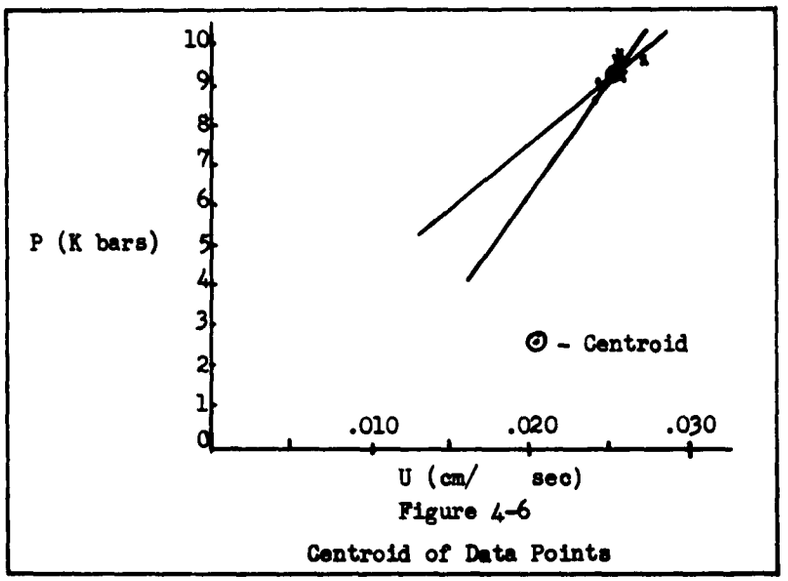

Figure 4-6

Centroid of Data Points

Discussion of Discrepancies

Several errors for which a relative magnitude cannot be fixed are omitted from the error analysis. This does not mean they are not present or considered, but that they cannot be calculated. The primary error of this type is obtained in using the data reduction equipment. The machine used eliminated the error of incorrect reading of the magnitudes of the data but still required proper alignment by the observer to obtain these readings. The human error of "eye-ball" alignment is consequently introduced. It is further assumed that the scope had a constant sweep speed and that the vertical deflection of the voltage trace was linear.

The time delay in the transmission lines produces an error in time measurements. This error is eliminated by measuring the time delay in these lines and determining a correction factor. This correction factor is applied to all time measurements to give true time measurements.

Assuming the transmission factor, α, as defined in Eq (7), is not truly correct. α is determined from properties with zero particle velocity (i.e. Co_q and Co) where the particle velocity in the sample is not zero. Since particle velocities are low, Co is not greatly effected and this assumption then is quite reasonable.

Two sample materials, OTWR and teflon, gave non-uniform results when the values of P, U, and η obtained from the deceleration method and the quartz method are compared. The first discrepancy, OTWR, is explained in the following discussion.

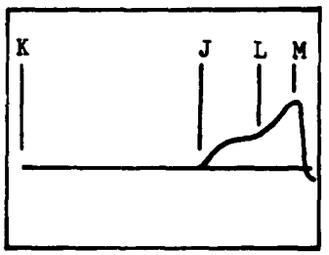

Figure 4-7

Trace of Wave Transit Time for OTWR

The transit time of the shock wave through the sample was represented by the distance KL. However, the pressure was read at a later time at point M. The part of the pressure profile represented by JL is called a precursor, or a fore-running disturbance which arrives before the actual elastic wave. There is no distinct elastic wave front so no definite point can be tied down for L. Therefore, the wave transit time is not precisely known and L could be anywhere between J and M.

To obtain a value of wave transit time, L is assumed to be at the point of curvature change of the precursor to elastic wave. This assumption gives higher values of particle velocity in the deceleration method than the values obtained from the quartz method. This is due to a measured longer transit time than is indicated by the quarts results, and yields a smaller D. This in turn decreases the slope of the straight line plot of P vs U from Eq (2) and shifts the intersection A shown in Fig 4-4 to the right. In shifting A to the right, a higher particle velocity is obtained. The plot of D vs U for OTWR in Fig D-9 shows this characteristic.

The discrepancies in teflon observed in Fig D-16, Fig D-17, and Fig D-18 can only be explained in the following manner. The teflon samples used in the shots were extras that were not used in a prior, similar experiment. They did not exactly fit the holders and pressure was used to set them in the holders seemingly flush with the front face.

This was not ideal and several of the transducer were found not to have a flush front face. This discrepancy was not observed in any of the other samples. Once a sample has been potted in the lucite holder, it is not feasible to recover the sample and so the transducers were fired, knowning that the front surface was not flush. This variance would account for the spread of values for the teflon shots.

Bibliography

1. Cook, Nathan H. and Ernest Rabinowics. Physical Measurement and Analysis. Reading, Massachusetts: Addison-Wesley Publishing Company, Inc., 1963.

2. Courant, R. and K. O. Friedricks. Supersonic Flow and Shock Waves. Baltimore: Waverly Press, 1948.

3. Duvall, G. E. Some Properties and Applications of Shock Waves. SRI Project No. GU-2912. Menlo Park, California: Stanford Research Institute, 1960.

4. Fowles, G. R. "Shock Wave Compression of Hardened and Annealed 2024 Aluminum". Journal of Applied Physics, 32:1475-1488. (August 1961).

5. Fry, W. J., J. M. Taylor, and Bertha W. Henuis. Design of Crystal Vibrating Systems. New York: Dover Publications, Inc., 1948.

6. Heising, Raymond A. Quartz Crystals for Electrical Circuits. New York: D. Van Nostrand Co., Inc., 1946.

7. Hund, August. Phenomena In High-Frequency Systems. New York: McGraw-Hill Book Company, Inc., 1936.

8. Jones, O. E., et al. "Dynamic Yield Behavior of Explosively Loaded Metals Determined by a Quartz Transducer Technique". Journal of Applied Physics, 33:3224-3233 (November 1962).

9. Kalsky, H. Stress Waves In Solids. London: Oxford University Press, 1953.

10. Lamberson, D. L., et al. Pressure Profile Measurements. POIR-1855. Kirtland AFB, New Mexico: Air Force Special Weapons Center, August 1962. (Secret-RD)

11. Rinehart, John S. "On Fractures Caused by Explosions and Impacts". Quarterly of the Colorado School of Mines, 55 (October 1960).

12. Rocard, Yves. General Dynamics of Vibrations. New York: Frederick Ungar Publishing Co., 1960.

13. Smith, J. H. and L. M. Barker. Measurement of Tilt, Impact Velocity, and Impact Times Between Two Plane Surfaces. SC-4728(RR). Albuquerque, New Mexico: Sandia Corporation, December 1962.

14. Wagner, M. H., et al. Determination of Hugoniot Equation-of-State for Polymers and Re-Entry Vehicle Materials and Investigations of Fracture Phenomena. AFSWC-TDR-62-66. Downey, California: Aerojet-General Corporation, August 1962.

Appendix A

Transverse Wave Effects

One of the assumptions made in this thesis is that the pressure incident on the face of the quarts crystal is the pressure generated by the longitudinal shock wave. This is a valid assumption as will be shown.

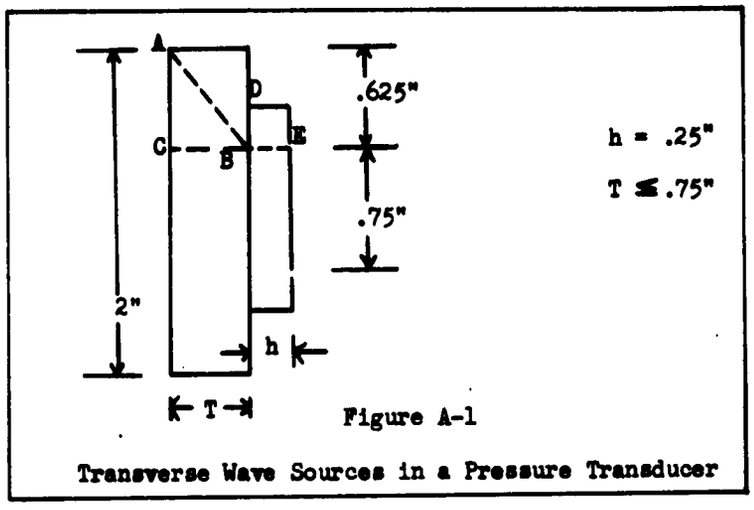

Figure A-1

Transverse Wave Sources in a Pressure Transducer

Fig A-1 shows two possible sources of transverse waves that might effect the pressure on the inner electrode. The first would be a disturbance generated at A propagating to B. To be a disturbance, the transit time t_{AB} would have to be less than the transit time t_{CE}.

Assuming that the transverse and longitudinal wave propagation velocities are equal in the sample, and knowing the wave propagation velocity in quartz, the transit time between points A and B is given by:

$$t_{AB} = \frac{AB}{v_x} = \frac{\sqrt{t^2 + (5/8)^2}}{v_x} \qquad \text{(A-1)}$$

The transit time between points C and E is given by:

$$t_{CE} = t_{CB} + t_{BE} = \frac{t}{v_x} + \frac{1/4}{v_q} \qquad \text{(A-2)}$$

Squaring both t_{AB} and t_{CE} and substracting the two resulting quantities yields:

$$t_{AB}^2 - t_{CE}^2 = \frac{t^2}{v_x^2} + \frac{25/64}{v_x^2} - \left(\frac{t^2}{v_x^2} + \frac{t/4}{v_x v_q} + \frac{1/16}{v_q^2}\right) \qquad \text{(A-3)}$$

But since $v_q > v_x$, then

$$t_{AB}^2 - t_{CE}^2 = \frac{25/64}{v_x^2} - \frac{16t/64}{v_x^2} - \frac{4/64}{v_x^2} \qquad \text{(A-4)}$$

This reduces to:

$$t_{AB}^2 - t_{CE}^2 = \frac{21 - 16t}{64\, v_x^2} \qquad \text{(A-5)}$$

Hence, for $t < \frac{21"}{16} \sim 1.25"$, $t_{AB} > t_{CE}$ and no transverse wave effects are introduced from the source at A.

The second source also shown in Fig A-1, a disturbance at D propagating to B, is eliminated by the guard rings. Again, if the assumption that the transverse wave velocity in quartz is the same as the longitudinal wave velocity in quartz is valid, then the time for the disturbance to propagate from D to B, is t_{DB}. By cutting the guard rings such that the distance DB is the same as the thickness, h, of the crystal or distance BE, then the wave will have propagated through the crystal and measurements taken before the transverse wave from D arrives at B.

From the previous discussion, the assumption that there are no transverse shock wave effects - or that the pressure incident on the quartz is one dimensional - is valid.

Appendix B

Guard Rings

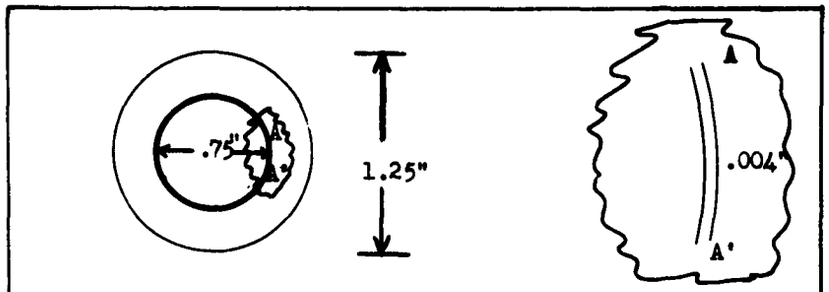

Figure B-1

Quartz Crystal With Guard Ring

Guard rings are cut for the purpose of elimination of transverse pressure effects as discussed in Appendix A. Where this eliminates a certain undesirable effect, it generates a new problem.

The current generated by the crystal is proportional to the area and the pressure incident on it. The area of the two electrodes formed by the guard rings is not equal. As the transverse pressure builds up in the outside electrode, the pressure incident on the two electrodes is not equal.

The solution desired is that the current produced, and consequently the voltage ($V = i \cdot R_s$), by the two electrodes be equal. This eliminates arcing between the electrodes. To approximate this condition, the pressure is assumed to be constant on both electrodes (i.e. neglected the effects of the transverse waves in the outer electrode). Hence, the voltage is directly proportional to the product of the area of the electrodes and their respective resistances as shown in Fig B-2.

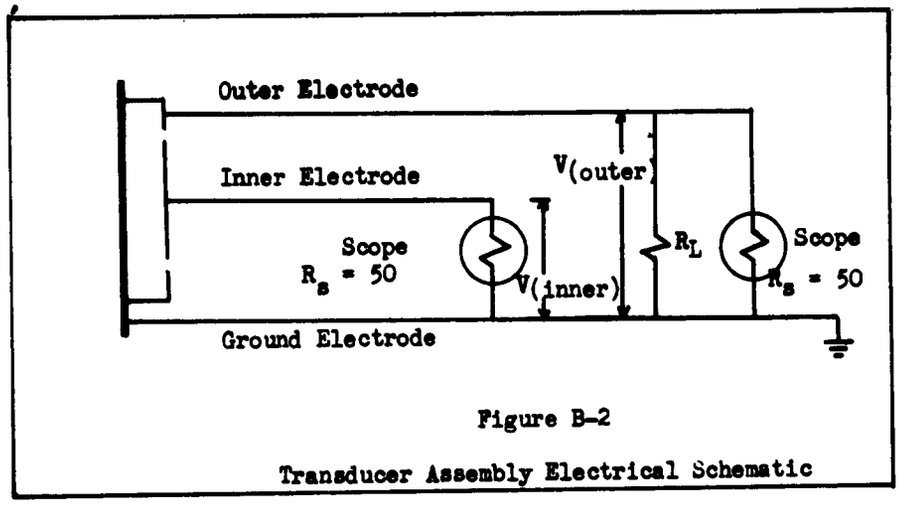

Figure B-2

Transducer Assembly Electrical Schematic

Eq (B-1) puts this condition into an equation:

$$A_{(in)}\ R_{(in)} = A_{(out)}\ R_{(out)} \qquad \text{(B-1)}$$

$$\frac{\pi\,(.75")^2}{4} \cdot 50\Omega = \frac{\pi\,((1.25")^2 - (.75")^2)}{4} \cdot R_{(out)}$$

$$R_{(out)} = 28.1\ \Omega$$

$R_{(out)}$ is obtained by placing a load resistor, R_L, in parallel with the scope to give the equilibrant resistance, $R_{(out)}$, desired. Eq (B-2) is solved for the value of R_L.

$$R_{(out)} = \frac{R_L\ R_s}{R_L\ R_s} \qquad \text{(B-2)}$$

$$R_L = \frac{R_s\ R_{(out)}}{R_s - R_{(out)}}$$

$$R_L = \frac{(50)(28.1)}{(50-28.1)} = 64.2\ \Omega$$

Pressure build-up during the first 0.3 μ sec is slight; so by taking the readings in this time interval, cutting guard-rings, and using a load resistor, most of the extraneous errors in the technique are eliminated.

Appendix C

Pressure Vs Particle Velocity Curve for AL-6061-T6

The curve plotted in Fig C-1 on the following page was plotted from points tested below in Table C-1. The low pressure points are obtained from data available at AFSWC. The high pressure points (i.e. above 34.9 then were obtained from (Ref 3:1483), which gives values for AL-2024. AL-6061-T6 does not vary appreciably from AL-2024 in this range. Also, only the sample material, gold, required the use of a curve above 15 K bar.

Table C-1
Values of P Vs U for AL-6061-T6

P (K bar)	U (cm/ μ sec)
1.58	.00095
2.42	.00145
4.42	.00265
5.20	.00310
5.32	.00315
7.12	.00423
9.58	.00592
10.01	.00623
11.50	.00727
13.76	.00872
14.32	.00901
15.53	.01001
34.9	.02105
37.1	.02235
39.1	.02360
41.1	.02480
43.1	.02600
45.0	.02710
47.5	.02860
49.3	.02955
50.9	.03045

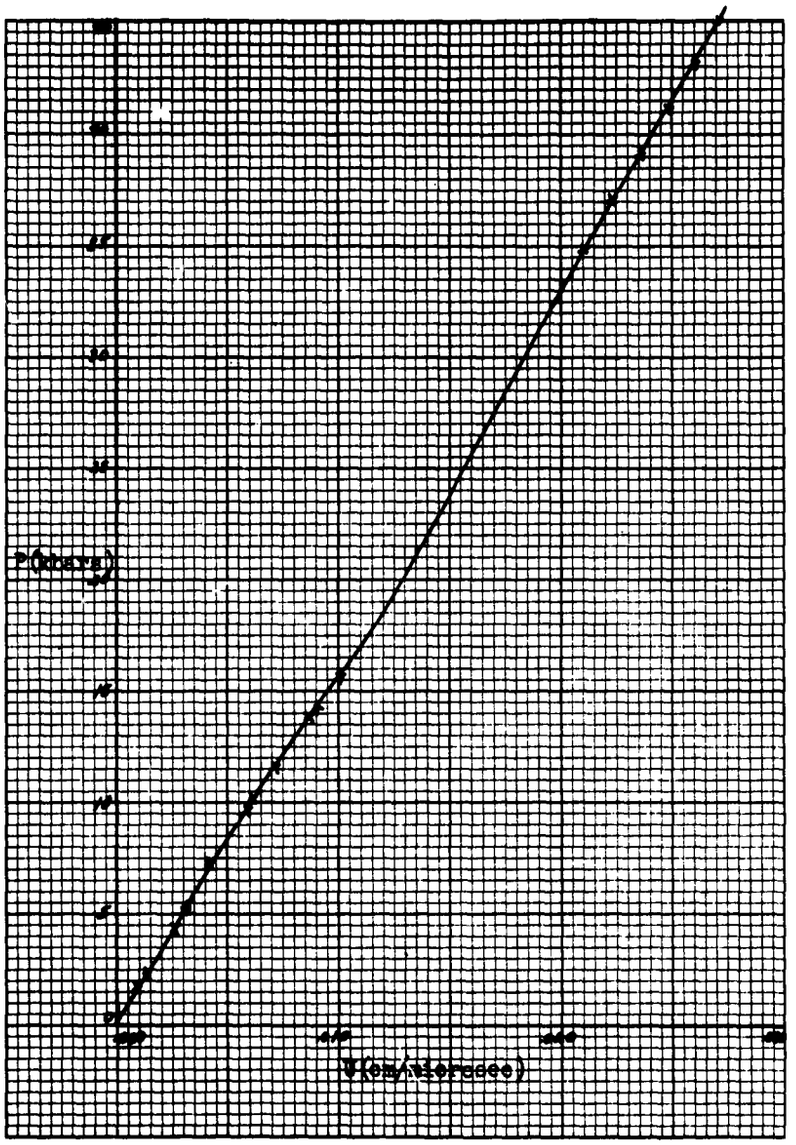

Fig C-1

P vs U Curve For AL 6061-T6

Appendix D

Tabulated and Graphical Result

The following table and graphs present the individual shot values of D, P, U, and η. The statistical errors in combining these points into a single point (i.e. centroid) is given along with the total error (i.e. $E_{tot} = (E_{exp}^2 + E_{se}^2)^{1/2}$). Each of the sample materials is treated separately and in the following order: C-124, CNP, OTWR, P-G, Au, and teflon.

Table D-1
Individual Shot Values of D, P, U, and η for C-124

D (cm/μ sec)	P (K bars)		U(cm/μ sec)		η	
	Decell Method	Quartz Method	Decell Method	Quartz Method	Decell Method	Quartz Method
.2874	8.59	9.218	.0241	.0259	1.092	1.099
.2874	8.59	9.511	.0241	.0267	1.092	1.102
.3035	9.09	9.653	.0242	.0256	1.087	1.092
.3035	9.09	9.640	.0242	.0256	1.087	1.092

Table D-2
Statistical Error for C-124

Plot	E_{se} %	E_{tot} %
P vs U	2.7	4.8
P vs η	4.2	5.8
D vs U	2.7	4.8

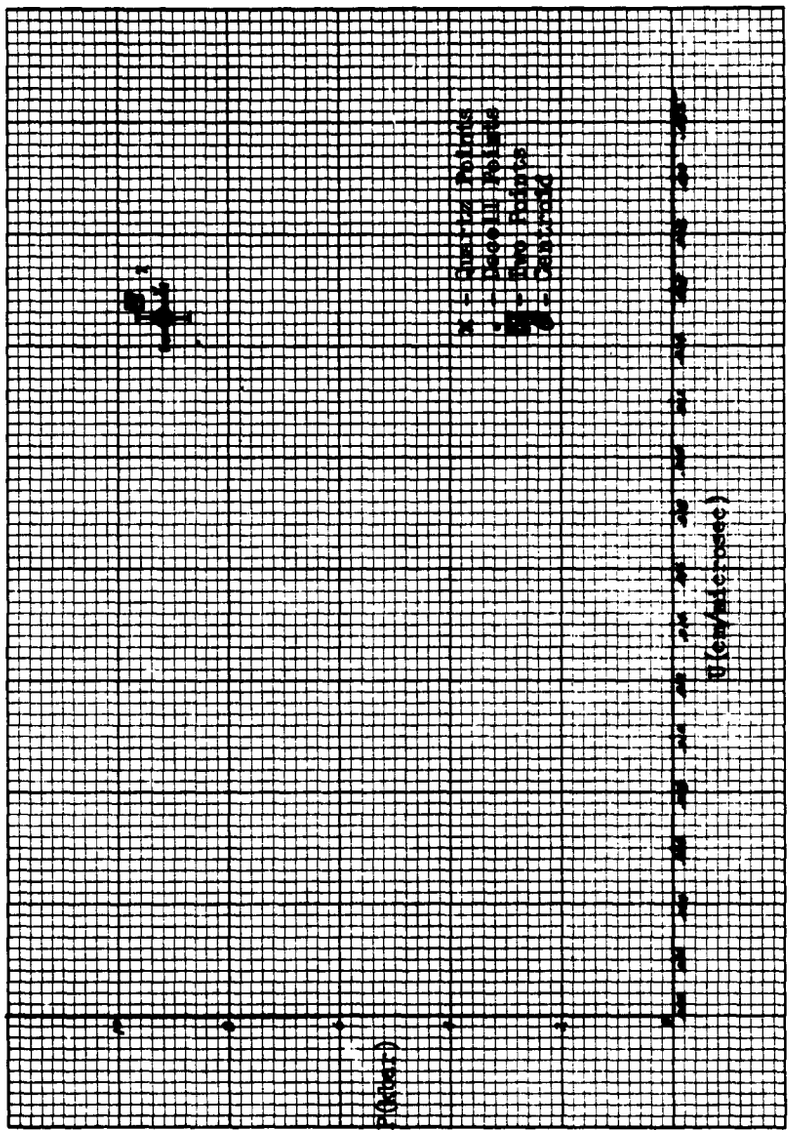

Fig D-1

P vs U Curve For C-124

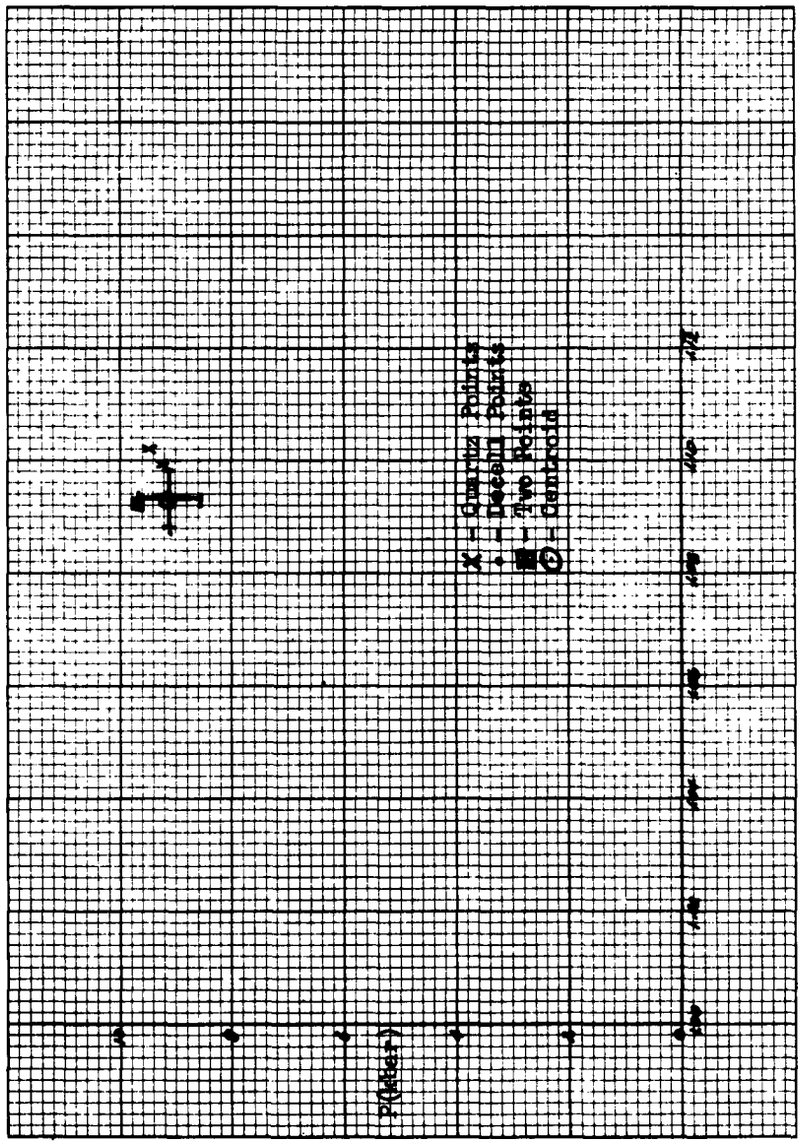

Fig D-2

P vs η Curve For C-124

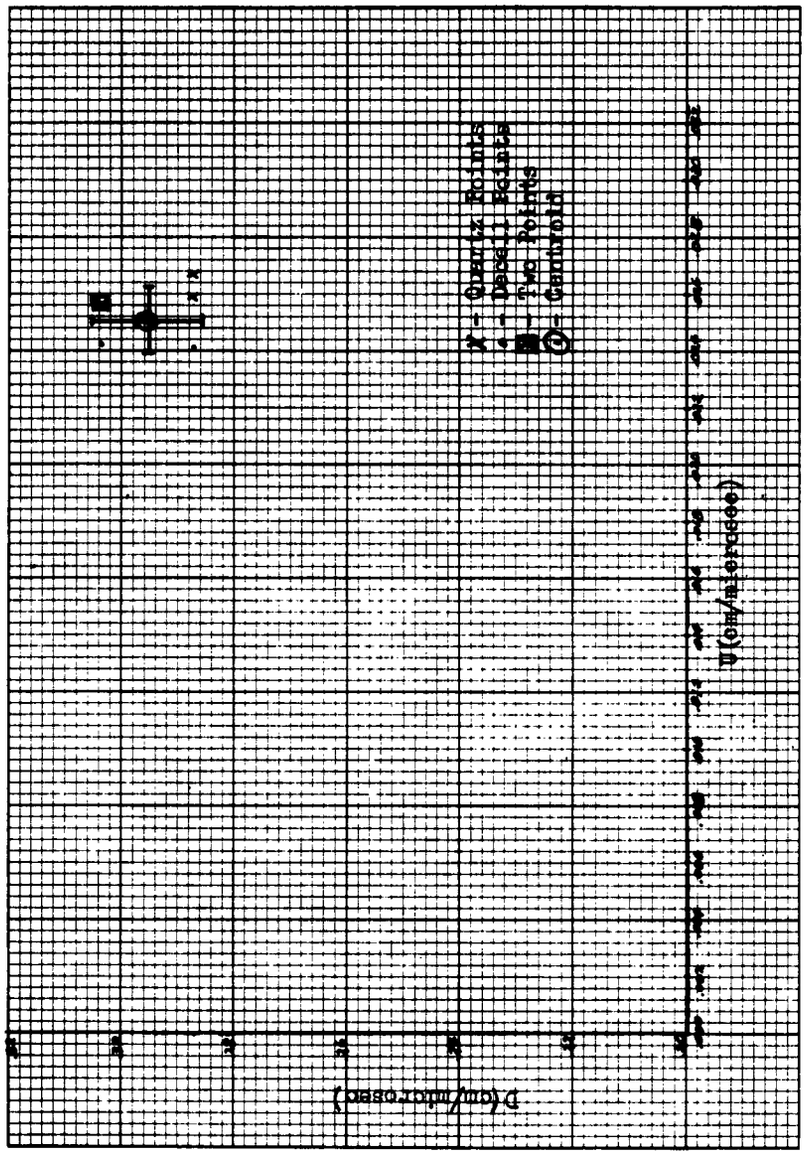

Fig D-3

D vs U Curve For C-124

Table D-3
Individual Shot Values of D, P, U, and η for CNP

D (cm/ μ sec)	P (K bars)		U(cm/ μ sec)		η	
	Decell Method	Quartz Method	Decell Method	Quartz Method	Decell Method	Quartz Method
.2716	7.88	5.571	.0241	.0171	1.097	1.067
.2541	7.82	8.768	.0258	.0288	1.113	1.128
.2732	8.03	8.629	.0245	.0263	1.098	1.107
.2984	7.60	8.603	.0213	.0240	1.077	1.088
.3067	8.80	8.349	.0240	.0227	1.085	1.080
.3067	8.80	9.539	.0240	.0259	1.085	1.092
.2811	8.84	8.578	.0236	.0254	1.091	1.099
.2811	8.84	8.275	.0236	.0245	1.091	1.096
.2801	8.75	8.431	.0241	.0251	1.094	1.098
.2801	8.75	8.800	.0241	.0262	1.094	1.103
.2974	8.61	8.516	.0243	.0239	1.089	1.087

Table D-4
Statistical Error for CNP

Plot	E_{se} %	E_{tot} %
[illegible] vs U	5.9	7.1
P vs η	8.1	9.0
[illegible] vs J	5.3	6.6

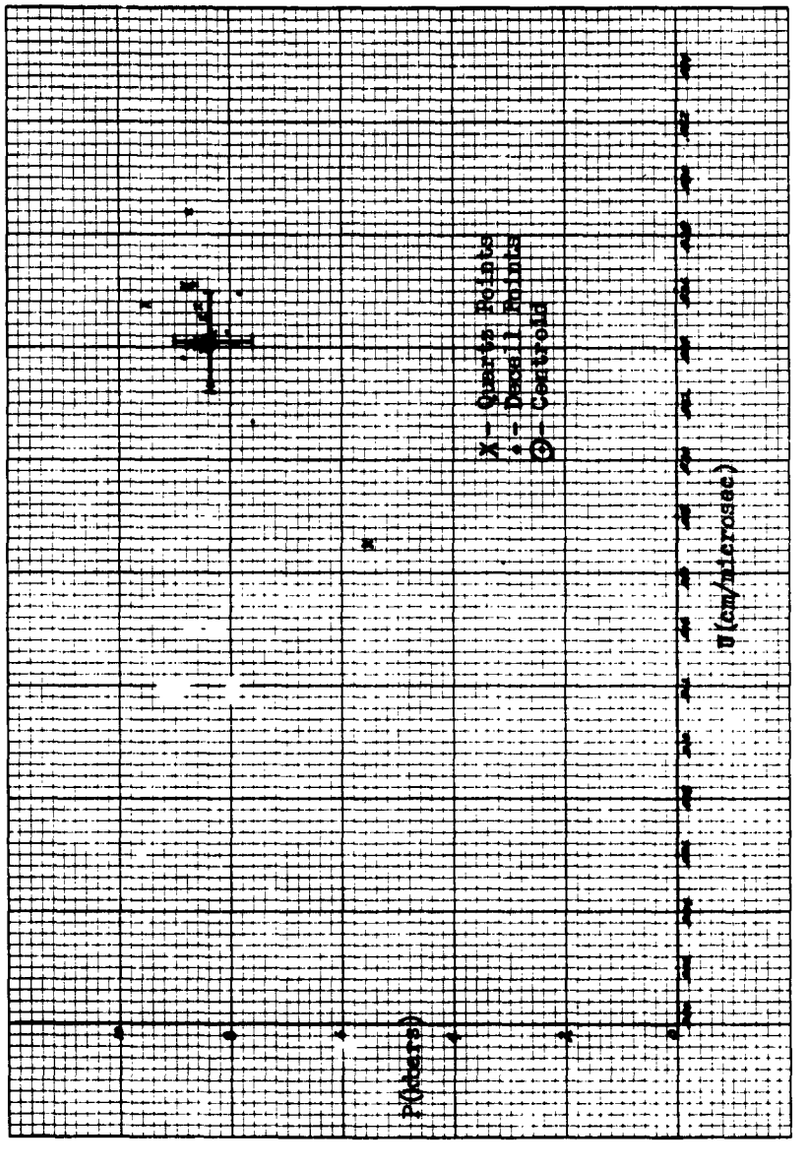

Fig D-4

P vs U Curve For CNP

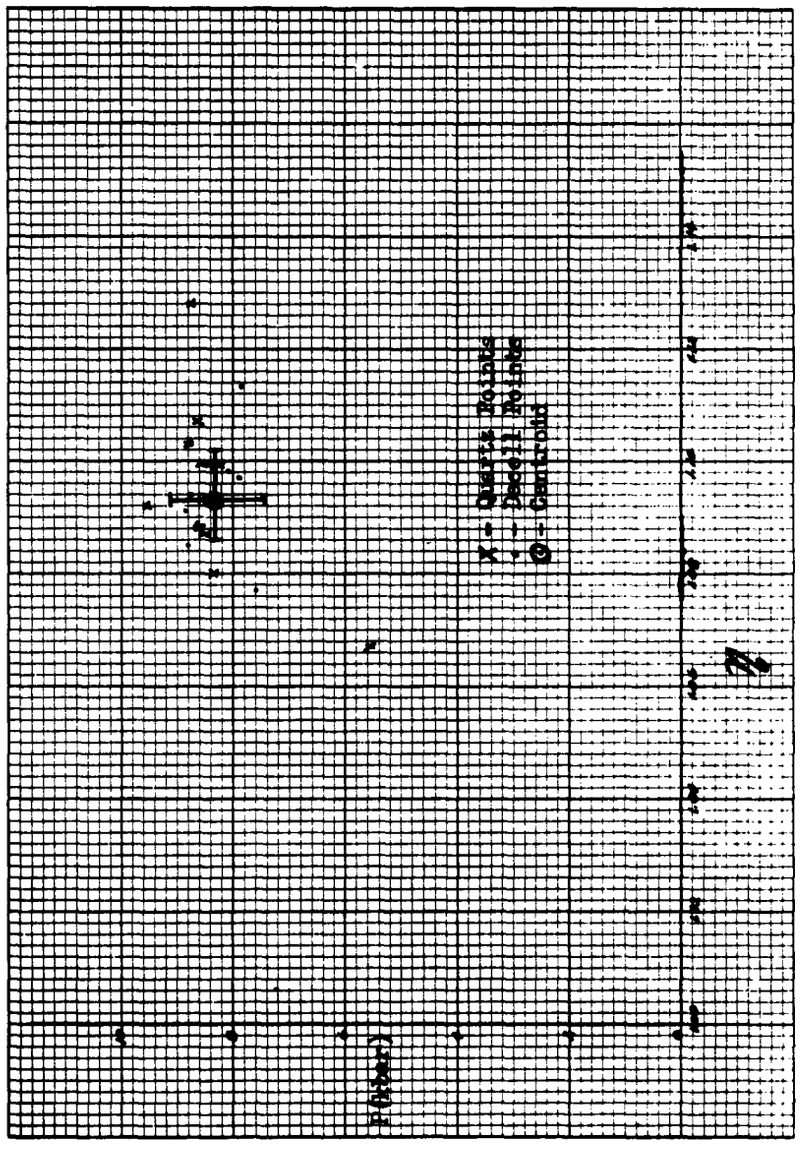

Fig D-5

P vs η Curve For CNP

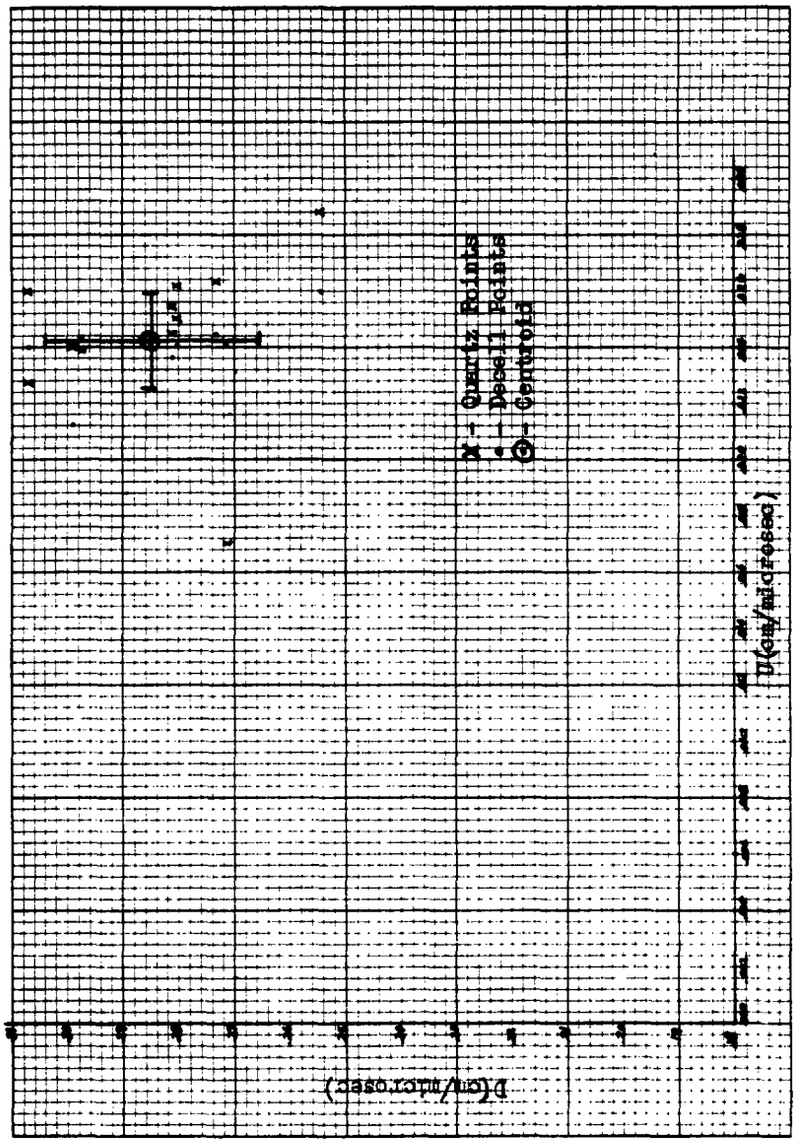

Fig D-6

D vs U Curve For CNP

Table D-5
Individual Shot Values of D, P, U, and ρ for OTWR

D (cm/μ sec)	P (K bars)		U(cm/μ sec)		ρ	
	Decell Method	Quartz Method	Decell Method	Quartz Method	Decell Method	Quartz Method
.2575	9.51	5.379	.0234	.0133	1.100	1.054
.2575	9.51	5.435	.0234	.0134	1.100	1.055
.2631	9.72	6.123	.0234	.0148	1.098	1.060
.2854	10.28	5.988	.0230	.0134	1.087	1.049

Table D-6
Statistical Error for OTWR

Plot	E_{se} %	E_{tot} %
P vs U	4.1	5.7
P vs ρ	8.5	9.4
D vs U	-	-

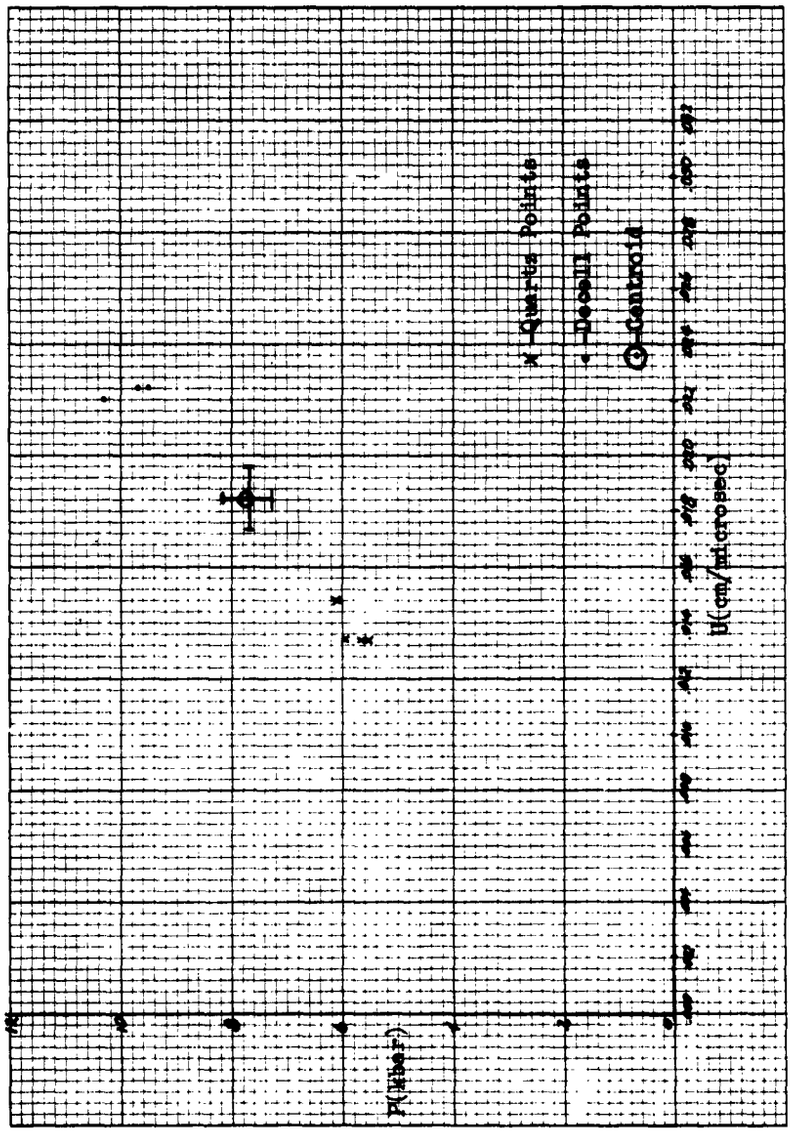

Fig D-7

P vs U Curve For OTWR

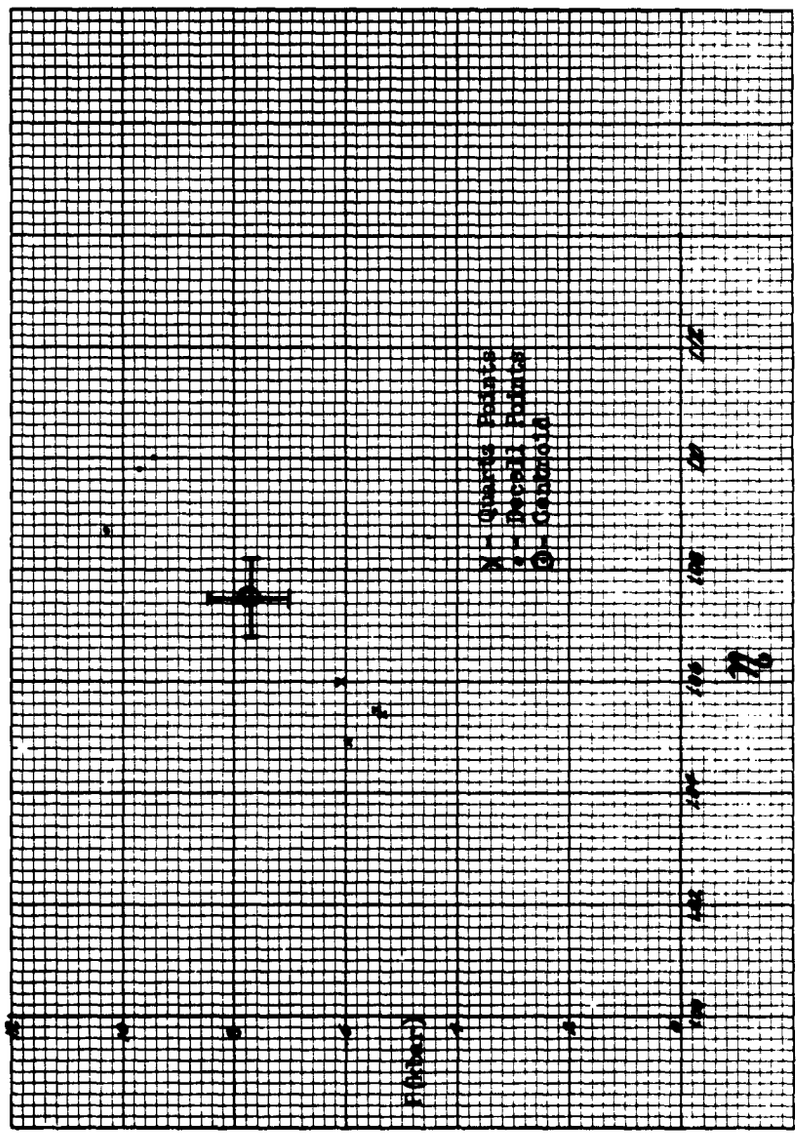

Fig D-8

P vs η Curve For OTWR

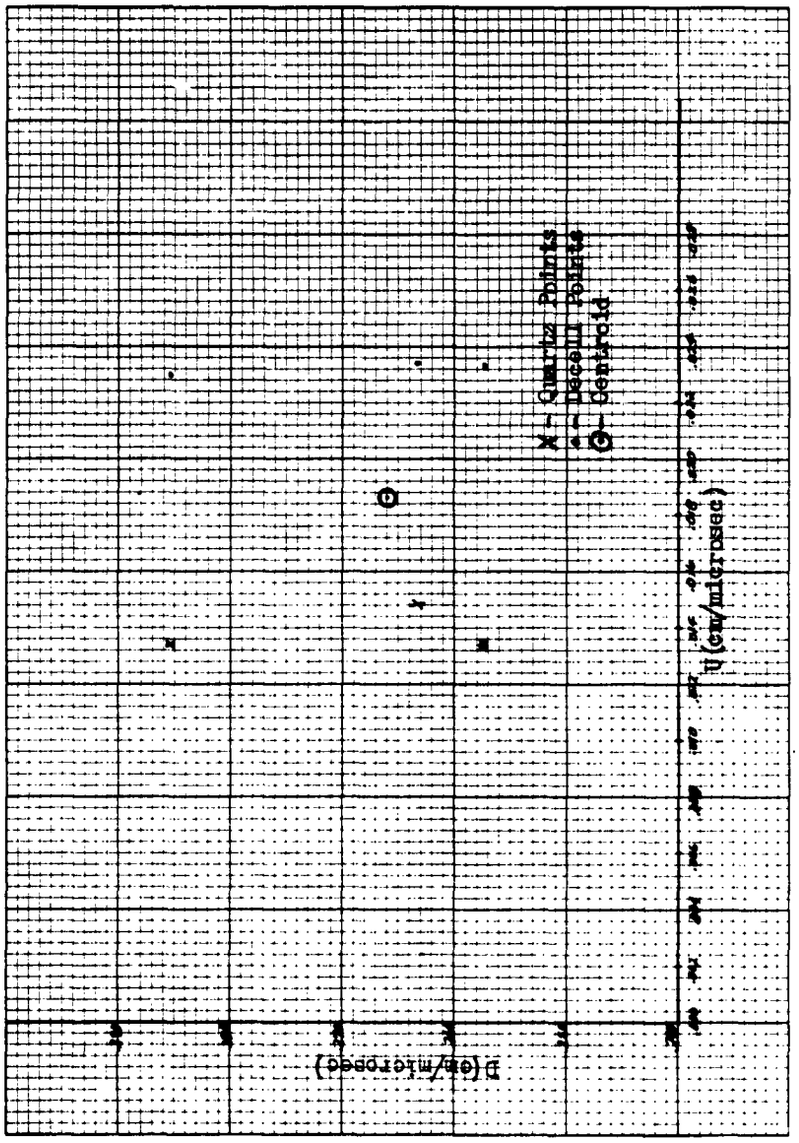

Fig D-9

D vs U Curve For OTWR

Table D-7
Individual Shot Values of D, P, U, and η for P-G

D (cm/ μ sec)	P (K bars)		U (cm/ μ sec)		η	
	Decell Method	Quartz Method	Decell Method	Quartz Method	Decell Method	Quartz Method
.4102	15.92	13.425	.0178	.0149	1.045	1.038
.4102	15.92	13.850	.0178	.0153	1.045	1.039
.3838	15.72	16.673	.0186	.0197	1.051	1.054
.3838	15.72	15.964	.0186	.0189	1.051	1.052
.3945	12.59	11.897	.0145	.0137	1.038	1.036
.3945	12.59	11.580	.0145	.0133	1.038	1.035

Table D-8
Statistical Error for P-G

Plot	E_{se} %	E_{tot} %
P vs U	2.4	4.7
P vs η	4.7	6.2
D vs U	2.6	4.8

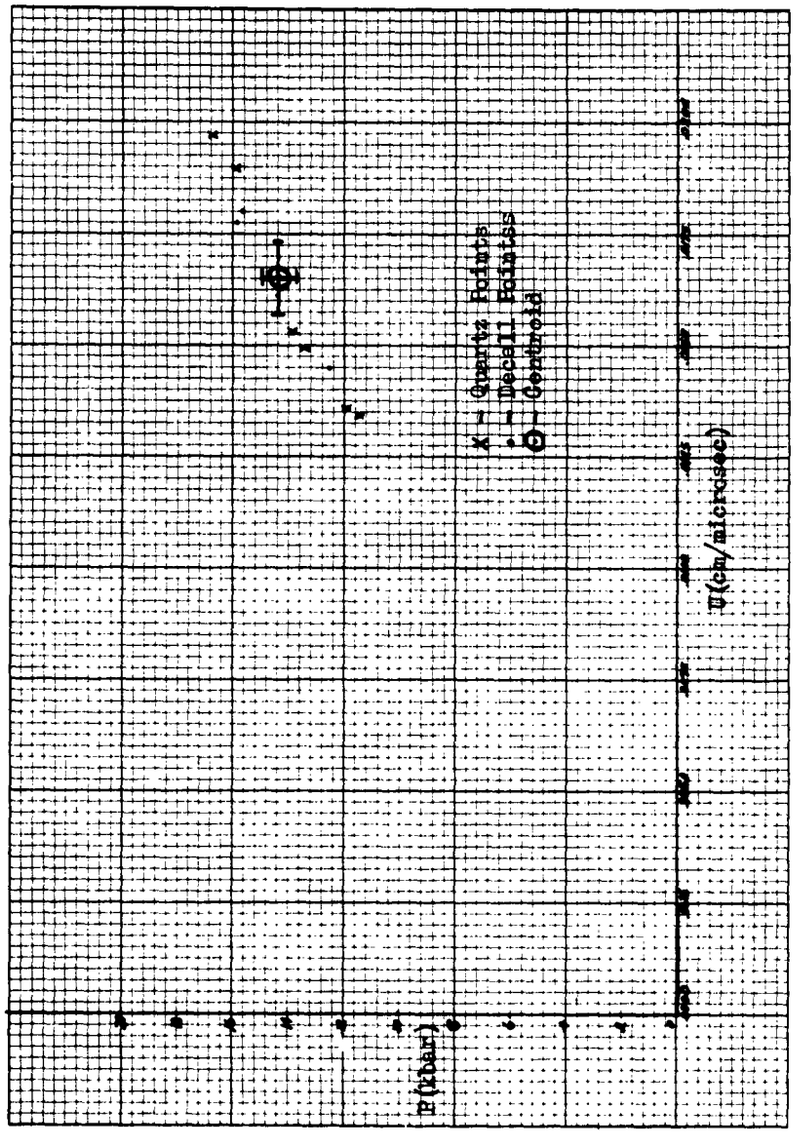

Fig D-10

P vs U Curve For P-G

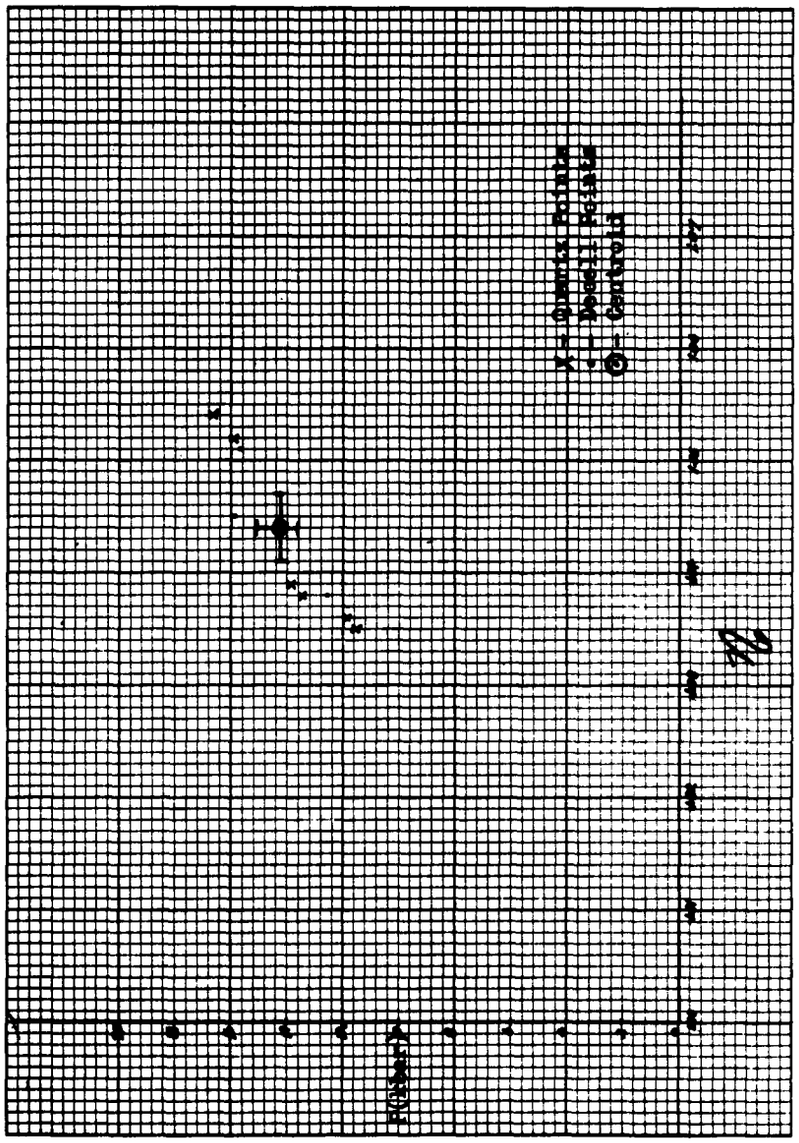

Fig D-11

P vs η Curve For P-G

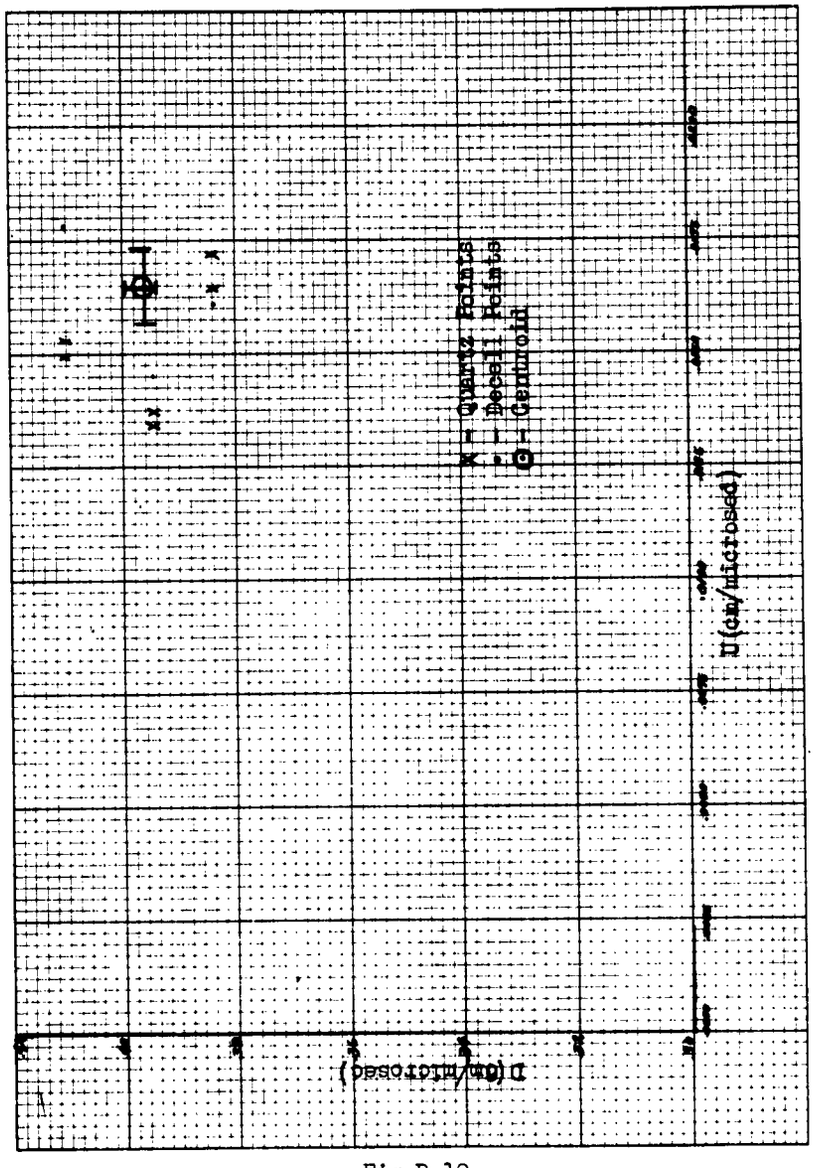

Fig D-12

D vs U Curve For P-G

Table D-9
Individual Shot Values of D, P, U, and η for Au

D (cm/ μ sec)	P (K bars)		U (cm/ μ sec)		η	
	Decell Method	Quartz Method	Decell Method	Quartz Method	Decell Method	Quartz Method
.3228	39.40	39.269	.0064	.0063	1.020	1.020
.3228	39.40	39.904	.0064	.0064	1.020	1.020

Table D-10
Statistical Error for Au

(Not Enough Values to Warrent a Statistical Error)

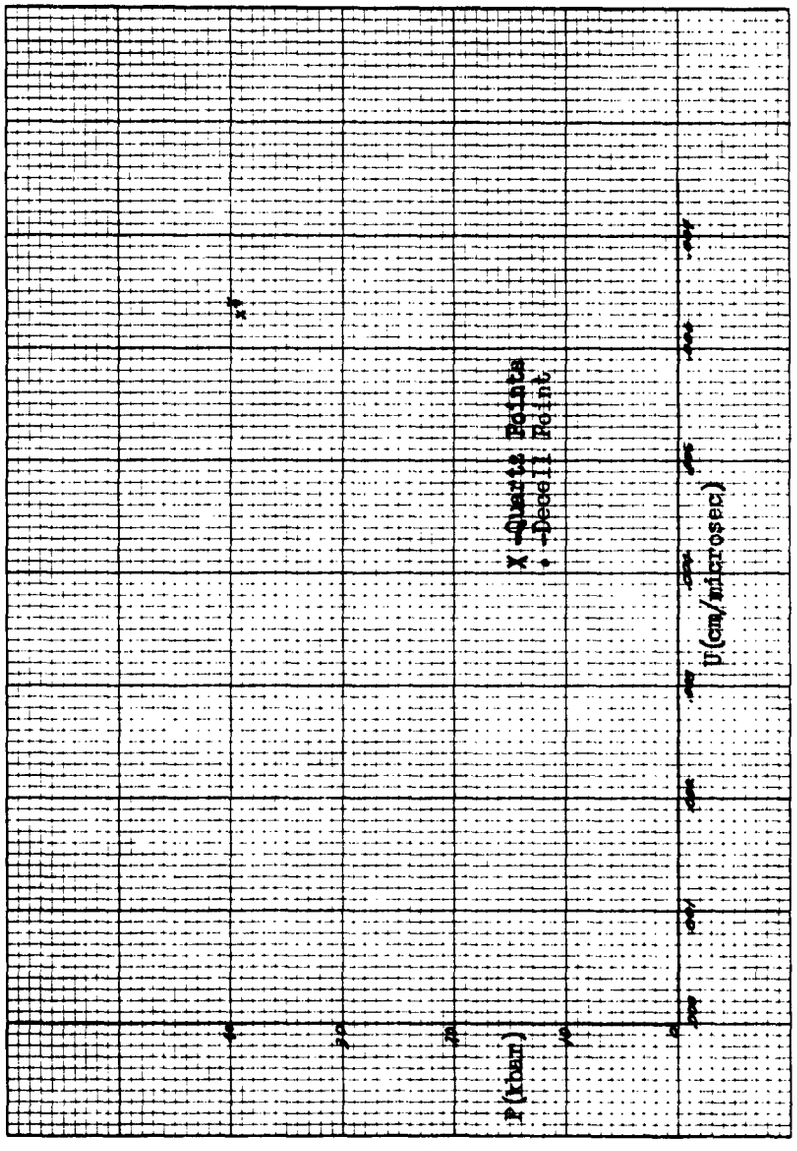

Fig D-13

P vs U Curve For Gold

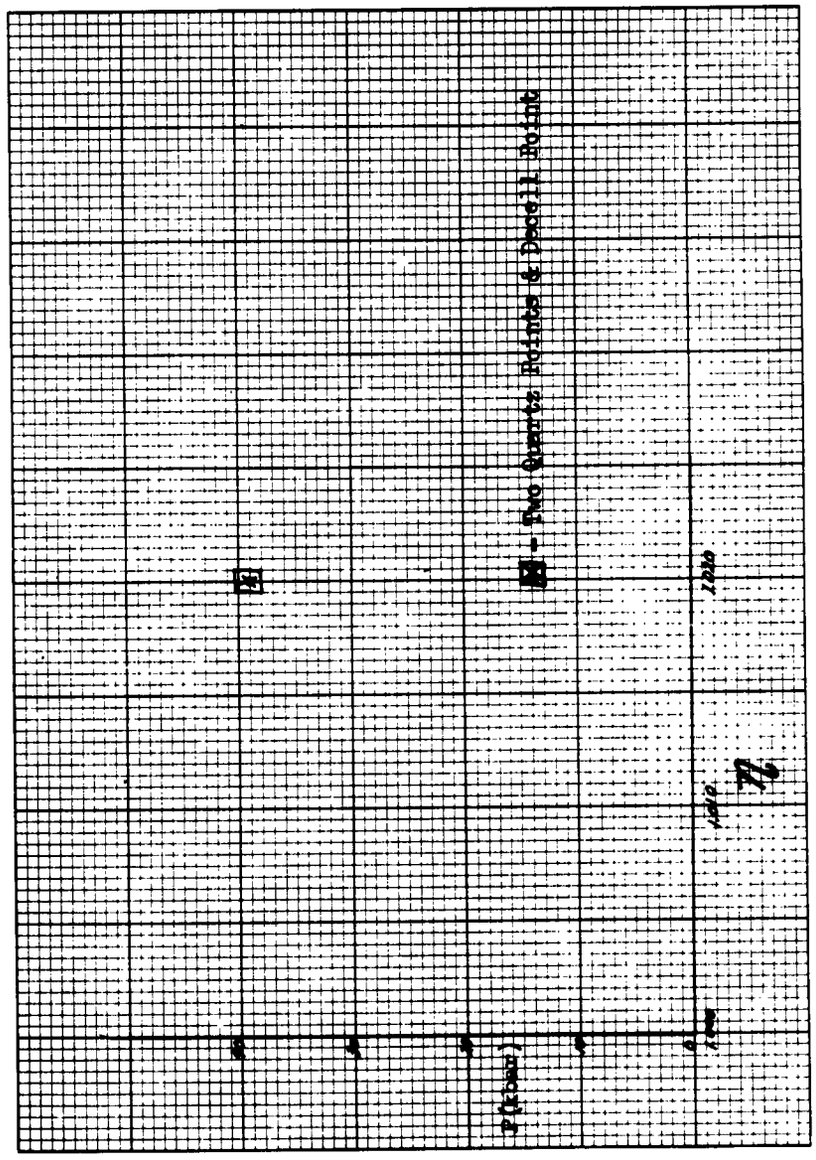

Fig D-14

P vs η Curve For Gold

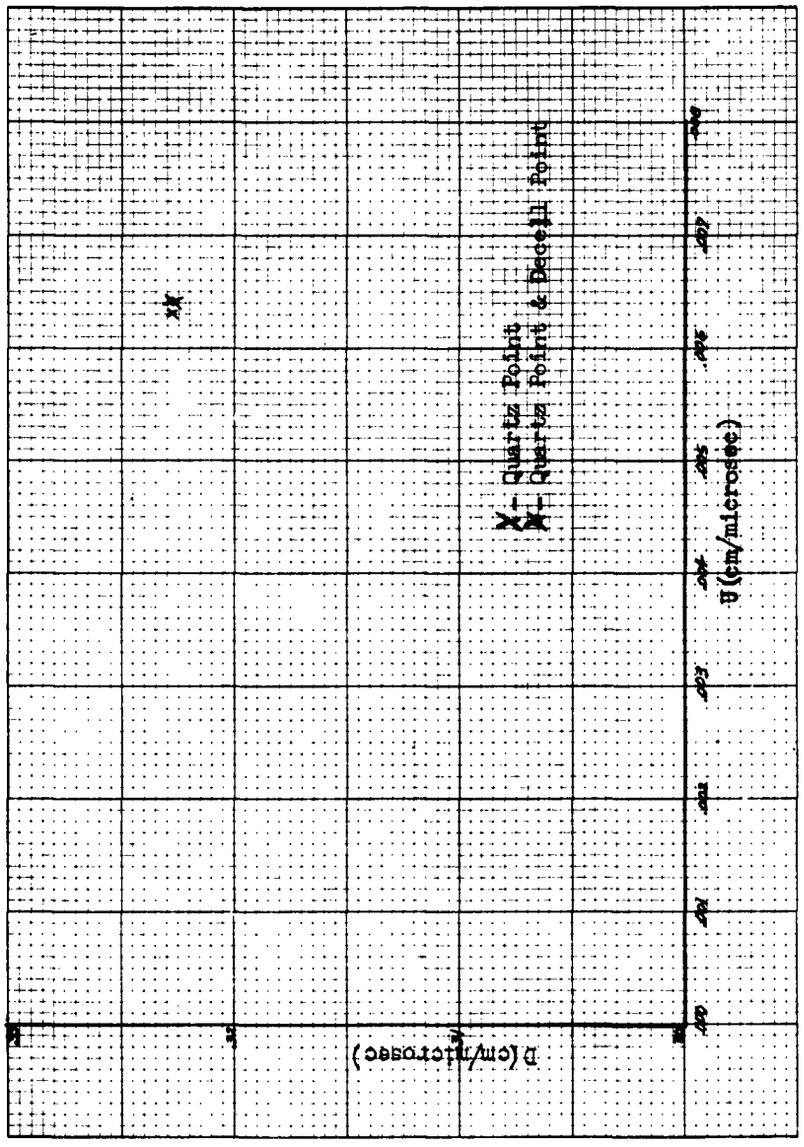

Fig D-15

D vs U Curve For Gold

Table D-11
Individual Shot Values of D, P, U, and η for Teflon

D (cm/μ sec)	P (K bars)		U(cm/μ sec)		η	
	Decell Method	Quartz Method	Decell Method	Quartz Method	Decell Method	Quartz Method
.1909	9.55	10.881	.0230	.0264	1.137	1.160
.1909	9.55	9.489	.0230	.0230	1.137	1.137
.1344	7.28	10.745	.0248	.0370	1.226	1.380
.1344	7.28	9.484	.0248	.0327	1.226	1.321
.2184	0.74	11.773	.0227	.0250	1.116	1.129
.2184	0.74	11.914	.0227	.0253	1.116	1.131.
.2449	1.79	11.477	.0222	.0217	1.100	1.097
.2449	1.79	11.498	.0222	.0217	1.100	1.097

Table D-12
Statistical Error for Teflon

Plot	E_{se} %	E_{tot} %
P vs U	13.9	14.5
P vs η	12.5	13.1
D vs U	14.9	15.4

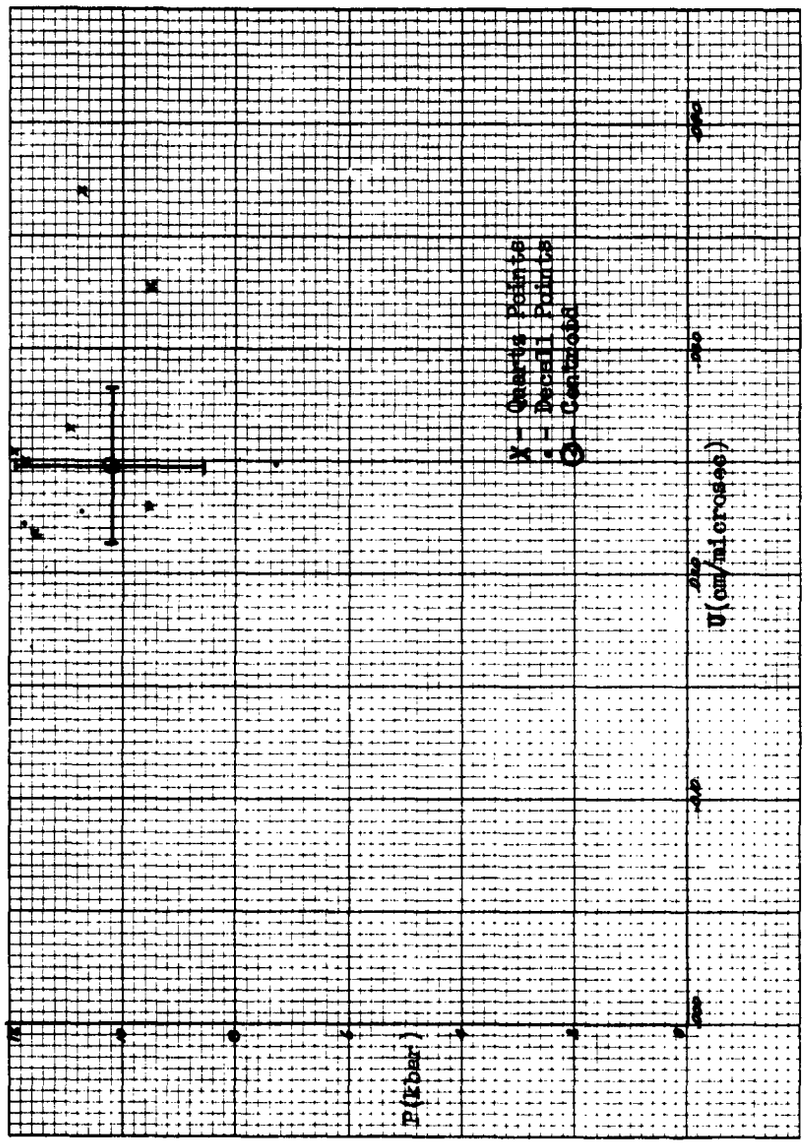

Fig D-16

P vs U Cnnve For Teflon

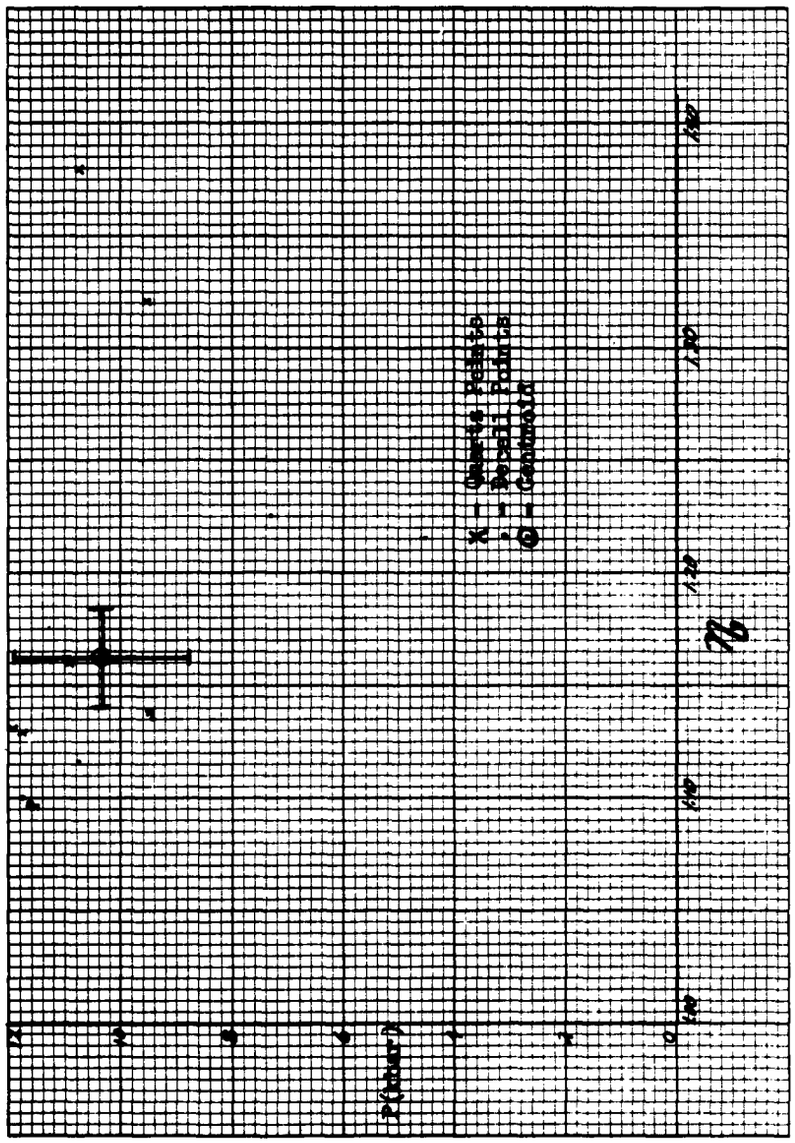

Fig D-17

P vs η Curve For Teflon

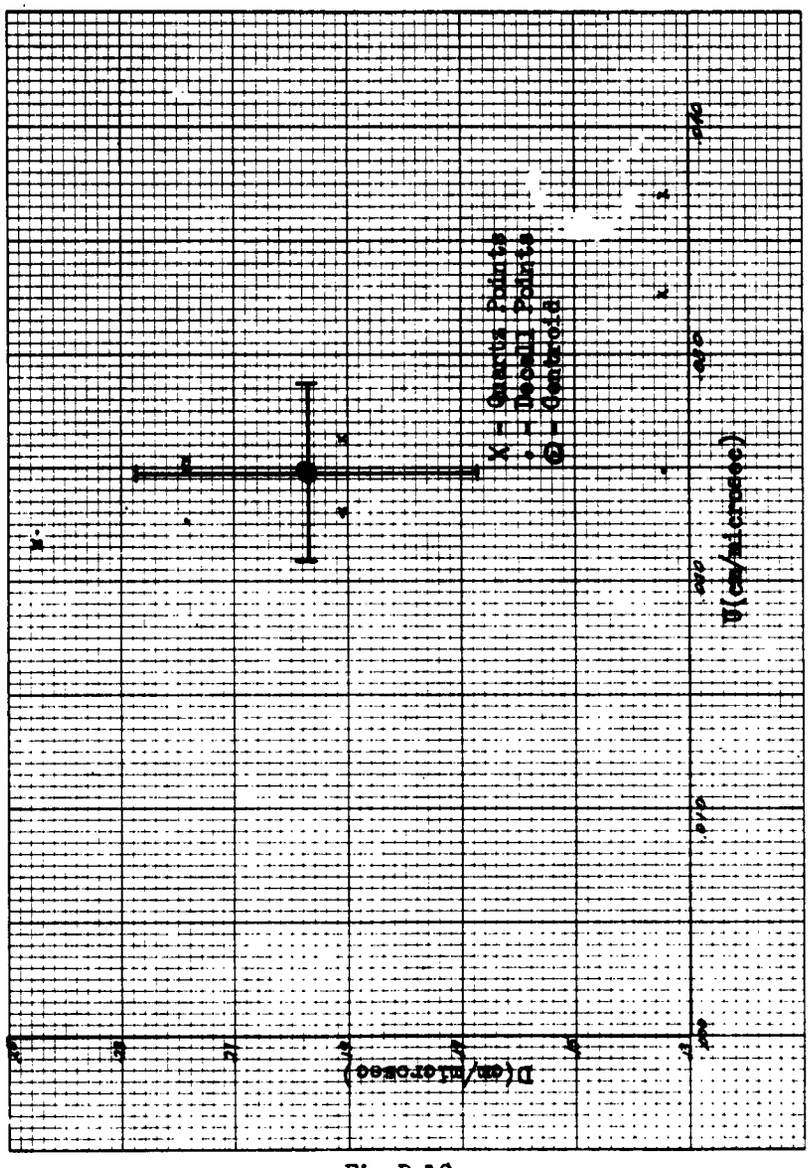

Fig D-18

D vs U Curve For Teflon

Appendix E

Constants and Measurements for Sample Calculations

Table E-1
General Constants

v_q	= .572 cm/ μ sec
K	= 2.16 X 10^{-8} coul/cm - K bar
o_q	= 2.65 gm/cm
C_{oq}	= .572 cm/ μ sec
o_{c-124}	= 1.24 gm/cm
C_{oc-124}	= .200 cm/ μ sec

Table E-2
Experimentally Determined Values

tt	= 2.58 μ sec
V	= 46.92 volts
W	= .02933 cm/ μ sec

Table E-3
Measured Parameters

T	= .7401 cm
G-R Dia	= 1.9036 cm
h	= .6412 cm
R_s	= 54 Ω